NASA/TM-2012-217772

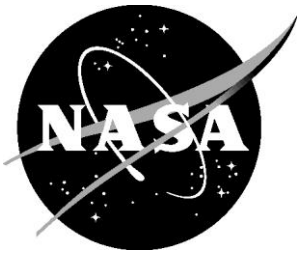

# Performance and Environmental Assessment of an Advanced Aircraft with Open Rotor Propulsion

*Mark D. Guynn*
*Langley Research Center, Hampton, Virginia*

*Jeffrey J. Berton, William J. Haller, Eric S. Hendricks, and Michael T. Tong*
*Glenn Research Center, Cleveland, Ohio*

October 2012

## NASA STI Program . . . in Profile

Since its founding, NASA has been dedicated to the advancement of aeronautics and space science. The NASA scientific and technical information (STI) program plays a key part in helping NASA maintain this important role.

The NASA STI program operates under the auspices of the Agency Chief Information Officer. It collects, organizes, provides for archiving, and disseminates NASA's STI. The NASA STI program provides access to the NASA Aeronautics and Space Database and its public interface, the NASA Technical Report Server, thus providing one of the largest collections of aeronautical and space science STI in the world. Results are published in both non-NASA channels and by NASA in the NASA STI Report Series, which includes the following report types:

- TECHNICAL PUBLICATION. Reports of completed research or a major significant phase of research that present the results of NASA Programs and include extensive data or theoretical analysis. Includes compilations of significant scientific and technical data and information deemed to be of continuing reference value. NASA counterpart of peer-reviewed formal professional papers, but having less stringent limitations on manuscript length and extent of graphic presentations.

- TECHNICAL MEMORANDUM. Scientific and technical findings that are preliminary or of specialized interest, e.g., quick release reports, working papers, and bibliographies that contain minimal annotation. Does not contain extensive analysis.

- CONTRACTOR REPORT. Scientific and technical findings by NASA-sponsored contractors and grantees.

- CONFERENCE PUBLICATION. Collected papers from scientific and technical conferences, symposia, seminars, or other meetings sponsored or co-sponsored by NASA.

- SPECIAL PUBLICATION. Scientific, technical, or historical information from NASA programs, projects, and missions, often concerned with subjects having substantial public interest.

- TECHNICAL TRANSLATION. English-language translations of foreign scientific and technical material pertinent to NASA's mission.

Specialized services also include organizing and publishing research results, distributing specialized research announcements and feeds, providing information desk and personal search support, and enabling data exchange services.

For more information about the NASA STI program, see the following:

- Access the NASA STI program home page at *http://www.sti.nasa.gov*

- E-mail your question to help@sti.nasa.gov

- Fax your question to the NASA STI Information Desk at 443-757-5803

- Phone the NASA STI Information Desk at 443-757-5802

- Write to:
  STI Information Desk
  NASA Center for AeroSpace Information
  7115 Standard Drive
  Hanover, MD 21076-1320

NASA/TM-2012-217772

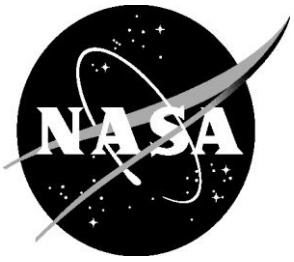

# Performance and Environmental Assessment of an Advanced Aircraft with Open Rotor Propulsion

*Mark D. Guynn*
*Langley Research Center, Hampton, Virginia*

*Jeffrey J. Berton, William J. Haller, Eric S. Hendricks, and Michael T. Tong*
*Glenn Research Center, Cleveland, Ohio*

National Aeronautics and
Space Administration

Langley Research Center
Hampton, Virginia 23681-2199

October 2012

## Acknowledgments

This study was supported by the Subsonic Fixed Wing project of NASA's Fundamental Aeronautics Program. Experimental data used in this study were obtained with support from the Environmentally Responsible Aviation project of NASA's Integrated Systems Research Program. Both this study and the open rotor wind tunnel test campaign were conducted in a collaborative partnership with General Electric Aviation.



Available from:

NASA Center for AeroSpace Information
7115 Standard Drive
Hanover, MD 21076-1320
443-757-5802

# Contents

## List of Tables

## List of Figures

## List of Acronyms, Symbols, and Abbreviations

$c_{Flight}$ – speed of sound at aircraft flight conditions

$c_{Tunnel}$ – speed of sound at wind tunnel test conditions

$D_p$ – mass of nitrogen oxides emitted over a standard landing-takeoff cycle

$D_{Full\text{-}Scale}$ – diameter of rotor for full scale engine

$D_{Rig}$ – diameter of rotor for wind tunnel model

$f_{Flight}$ – frequency of rotor noise at aircraft flight conditions

$f_{Static}$ – frequency of rotor noise at static conditions

$f_{Tunnel}$ – frequency of rotor noise at wind tunnel test conditions

$F_{oo}$ – engine rated output at sea-level, static conditions

$M$ – Mach number

$M_{Flight}$ – flight Mach number

$M_{Tunnel}$ – wind tunnel test Mach number

$SME$ – source motion exponent

$\alpha$ – aircraft angle of attack

$\alpha_{Cant}$ – rotor cant angle relative to aircraft zero angle of attack reference line

$\alpha_{Inflow}$ – rotor inflow angle

$\varepsilon$ – downwash angle at rotor location (angle of flow relative to freestream)

$\varepsilon_0$ – downwash angle at rotor location with aircraft angle of attack of zero

$\theta_G$ – geometric sideline microphone array angles

$\theta_E$ – noise emission yaw (polar) angles

$\rho_{Flight}$ – air density at aircraft flight conditions

$\rho_{Tunnel}$ – air density at wind tunnel test conditions

ACD – Acoustics Data Module

AFE – Above Field Elevation

ANOPP – Aircraft Noise Prediction Program

ASAT – Advanced Single-Aisle Transport

ASAT-or – Advanced Single-Aisle Transport-open rotor

ASAT-re – Advanced Single-Aisle Transport-rear engine (turbofan)

CSAT-re – Current technology Single-Aisle Transport-rear engine (turbofan)

EI – Emission Index, grams of emission per kilogram of fuel consumed

EPNL – Effective Perceived Noise Level

ERA – NASA Environmentally Responsible Aviation project

FAA – Federal Aviation Administration

FAR – Federal Aviation Regulations

FLOPS – Flight Optimization System

FPR – Fan Pressure Ratio

ICAO – International Civil Aviation Organization

ISA – International Standard Atmosphere

L/D – Lift-to-Drag ratio

LTO – Landing-Takeoff Cycle

NASA – National Aeronautics and Space Administration

$NO_X$ – Nitrogen Oxides (NO and $NO_2$)

NPSS – Numerical Propulsion System Simulation

OEW – Operating Empty Weight

PDCYL – Point Design of Cylindrical-bodied aircraft

PNL – Perceived Noise Level

PNLT – Perceived Noise Level, tone-corrected

SFW – NASA Subsonic Fixed Wing project

SL – Sea Level

SLS – Sea Level, Static

SPL – Sound Pressure Level

TOC – Top-Of-Climb

TSFC – Thrust Specific Fuel Consumption

T/W – Thrust-to-Weight ratio

WATE – Weight Analysis of Turbine Engines

# Abstract

*Application of high speed, advanced turboprops, or "propfans," to transonic transport aircraft received significant attention during the 1970s and 1980s when fuel efficiency was the driving focus of aeronautical research. Unfortunately, after fuel prices declined sharply there was no longer sufficient motivation to continue maturing this technology. Recent volatility in fuel prices and increasing concern for aviation's environmental impact, however, have renewed interest in unducted, open rotor propulsion and revived research by NASA and a number of engine manufacturers. Because of the renewed interest in open rotor propulsion, the lack of publicly available up-to-date studies assessing its benefits, and NASA's focus on reducing fuel consumption, a preliminary aircraft system level study on open rotor propulsion was initiated to inform decisions concerning research in this area. New analysis processes were established to assess the characteristics of open rotor aircraft. These processes were then used to assess the performance, noise, and emissions characteristics of an advanced, single-aisle aircraft using open rotor propulsion. The results of this initial study indicate open rotor engines have the potential to provide significant reductions in fuel consumption and landing-takeoff cycle $NO_X$ emissions compared to aircraft utilizing turbofan engines with equivalent core technology. In addition, noise analysis of the study configuration indicates that an open rotor aircraft in the single-aisle class would be able to meet current noise regulations with margin.*


## 1.0 Introduction

The Subsonic Fixed Wing (SFW) Project of NASA's Fundamental Aeronautics Program and the Environmentally Responsible Aviation (ERA) Project of NASA's Integrated System Research Program have jointly established a series of technology goals for future generations of subsonic transport aircraft. These goals are shown in Figure 1, where "N+*x*" refers to the series of technology generations which emerge over time. Propulsion technology will play a critical role in reaching the goals in every generation. Engines of the future will need to have lower fuel consumption, lower noise, and emit fewer harmful emissions. Airlines, and therefore aircraft and engine manufacturers, have always had a desire to reduce fuel consumption because of its direct impact on operating cost. But because of the significant risks inherent in adopting something completely new, a great deal of economic pressure is necessary for revolutionary technologies to be implemented. In NASA's opinion, however, the goals in Figure 1 cannot be achieved with conservative, evolutionary technologies and concepts. As NASA works towards these goals by investing in technology research and development, numerous unconventional ideas are considered and evaluated for their potential impacts. One such unconventional concept is open rotor propulsion.

| TECHNOLOGY BENEFITS* | TECHNOLOGY GENERATIONS (Technology Readiness Level = 4-6) | | |
|---|---|---|---|
| | N+1 (2015) | N+2 (2020**) | N+3 (2025) |
| Noise (cum margin rel. to Stage 4) | -32 dB | -42 dB | -71 dB |
| LTO NOx Emissions (rel. to CAEP 6) | -60% | -75% | -80% |
| Cruise NOx Emissions (rel. to 2005 best in class) | -55% | -70% | -80% |
| Aircraft Fuel/Energy Consumption‡ (rel. to 2005 best in class) | -33% | -50% | -60% |

* Projected benefits once technologies are matured and implemented by industry. Benefits vary by vehicle size and mission. N+1 and N+3 values are referenced to a 737-800 with CFM56-7B engines, N+2 values are referenced to a 777-200 with GE90 engines

** ERA's time-phased approach includes advancing "long-pole" technologies to TRL 6 by 2015

‡ $CO_2$ emission benefits dependent on life-cycle $CO_{2e}$ per MJ for fuel and/or energy source used

Figure 1. NASA's technology goals for subsonic transport aircraft.

When the aviation industry faced dramatically rising fuel costs in the 1970s, the response was a national research portfolio aimed at improving aircraft fuel efficiency (refs. 1, 2). One element of this research portfolio was the NASA Advanced Turboprop Project, focused on high-speed, unducted (or "open rotor") propulsors (ref. 3). A number of open rotor concepts were developed and tested as part of this program. The program was highly successful and was awarded the Collier Trophy in 1987; but after fuel prices declined sharply there was no longer sufficient motivation to continue maturing the technology and the ducted turbofan engine continues to be the standard propulsion system for high-speed commercial transport aircraft. However, recent volatility in fuel prices and increasing concern for aviation's environmental impact have renewed interest in unducted, open rotor propulsion for airliners and revived research by NASA and a number of engine manufacturers (refs. 4, 5).

Numerous studies on the benefits of open rotor engines were conducted in the 1970s and 1980s; references 6 and 7 describe two of many examples. Generally, the target applications in these studies were short range aircraft in the 100-150 passenger class with cruise Mach numbers less than 0.8. The fuel consumption benefit of open rotor propulsion compared to equivalent technology turbofan engines was typically found to be around 25%. One of the challenges consistently identified, however, was higher noise. Interior noise was reduced to levels equivalent to aircraft of that era through the use of additional fuselage acoustic treatment, at the cost of increased aircraft empty weight. Most of the studies found certification noise levels at or below FAA Stage 3/ICAO Chapter 3 limits (see references 8 and 9 for a description of aircraft noise certification). Although commercial transport aircraft designs with open rotor propulsion were studied extensively in the past, the results of those studies do not necessarily remain valid today due to advances in airframe and engine technology, and changes in the regulatory and market environments into which the aircraft will be inserted. Benefits measured relative to the engines of that era are no longer valid since ducted turbofan engines have advanced in the intervening years. Also, current and future noise regulations are stricter than those considered in the past studies. Because of the renewed interest in open rotor propulsion, the lack of publicly-available up-to-date studies assessing its benefits, and NASA's focus on reducing fuel consumption, internal NASA studies on open rotor propulsion were initiated to inform decisions concerning research in this area. These system-level studies leverage an open rotor research partnership between General Electric Aviation and NASA's Environmentally Responsible Aviation Project.

Unfortunately, in the two decades that have passed since open rotor concepts were thoroughly investigated, NASA has lost experience and expertise in this technology area. In order for an open rotor aircraft to be assessed to the same level of confidence as more traditional designs, new tools and methods are needed. The first step in performing a reliable assessment of this technology is to develop the necessary analysis processes. This report describes the initial capabilities which have been established in the SFW project to assess aircraft-level characteristics for designs with open rotor propulsion. Many of these open rotor specific analysis procedures were developed in cooperation with General Electric Aviation. The results of an aircraft system level assessment of open rotor propulsion applied to a Boeing 737/Airbus 320 class vehicle are then presented and compared to those for an equivalent technology geared turbofan based design. A potential new vehicle in this size class would be a prime candidate for open rotor propulsion because the 737/A320 class represents a significant portion of the global airline fleet, and a significant opportunity for technology insertion. Sixty-nine percent of the new aircraft produced over the next 20 years are projected to be in this class (ref. 10). Advances made to reduce the fuel consumption, noise, and emissions of these aircraft could provide a considerable positive contribution to the goal of minimizing the future environmental impact of aviation.

# 2.0 Study Objectives and Approach

This is a preliminary study with the objective of assessing the potential benefits and penalties of open rotor propulsion concepts as applied to an advanced 737/A320 replacement aircraft. This initial study is necessarily limited in detail and scope due to a lack of analysis tools to address all aspects of open rotor propulsion design, performance, and integration. Models used are approximate and the results should be viewed as preliminary while enhancements to the methods and data used to feed the processes continue. The general approach taken for this study is to develop analytical models of advanced engines, combine them with an advanced technology airframe, design the overall system to meet mission requirements and constraints, and assess the resulting noise, fuel consumption, and emission characteristics.

# 3.0 Modeling and Analysis Methodology

## 3.1 Propulsion Modeling

Propulsion system modeling was performed using the Numerical Propulsion System Simulation (NPSS) code (refs. 11-13) for thermodynamic cycle analysis and performance and the Weight Analysis of Turbine Engines (WATE) code (refs. 14-16) for aeromechanical design and weight estimates. Estimates for emission of nitrogen oxides ($NO_X$) were obtained from an empirical correlation representing an advanced, low-$NO_X$ combustor. Reference 17 provides more details on this empirical $NO_X$ correlation, which was developed by NASA combustor technologists during the latter stages of NASA's Ultra-Efficient Engine Technology Program. Developing the capability to design and analyze open rotor engines with NPSS was a significant task in itself. A new counter-rotating propeller performance element was added to NPSS to enable proper modeling. To model rotor performance, performance maps were generated from experimental data obtained for a General Electric "Gen-1" rotor design at high speeds (NASA Glenn 8x6-ft Supersonic Wind Tunnel) and low speeds (NASA Glenn 9x15-ft Low-Speed Wind Tunnel). Although the capability to model both geared and direct drive open rotor engines was established in NPSS, a geared open rotor architecture has been assumed for this assessment based on an internal concept evaluation and input from General Electric. References 18 and 19 provide more details on the open rotor modeling approaches that have been recently developed. Engine technology assumptions for the current study were based on those used in the NASA advanced turbofan engine design studies described in references 17 and 20. Details on the analysis methodology for the geared turbofan engine model used as a comparison case in this study are also provided in references 17 and 20.

### 3.2 Airframe Modeling

Previous open rotor studies have identified a number of possible airframe integration options. Reference 21 contains an excellent discussion of the various propulsion system and integration options, and the benefits and issues associated with each combination. The primary focus toward the end of the open rotor work of the 1980s was the rear-mounted pusher configuration (see Figure 2). As detailed in reference 21, this integration approach is favored from the aspect of passenger accommodation (lower interior noise) and wing aerodynamics. Although there are a number of issues that would need to be addressed to make this configuration successful, such as foreign object damage susceptibility, stability and control impacts, and pylon wake-rotor interaction, this layout seemed to be the preferred approach during the late 1980s. Because NASA's current focus in open rotor propulsion is the counter-rotating, pusher concept and a rear-mounted installation is the most likely configuration for this propulsion system, a rear fuselage-mounted engine layout was selected for this initial study.

Figure 2. Rear-mounted open rotor pusher configuration, shown on Boeing 727 test vehicle.

Development of a suitable airframe analytical model began with modeling of a rear-engine, single-aisle MD-90-30 type configuration in the NASA aircraft sizing and synthesis code FLOPS (Flight Optimization System) (ref. 22). This model was developed using publicly-available data on weight and performance of the MD-90-30 (refs. 23, 24) and a NASA-developed engine model representative of the International Aero Engines V2525-D5 engine. The wing and fuselage structural weight estimates of FLOPS were replaced with estimates from PDCYL (ref. 25), which offers a less empirical, more analytical weight estimation methodology. Using geometry, weight (maximum gross weight and maximum landing weight), and mission data from reference 23, and wing weight and fuselage weight predictions from PDCYL, FLOPS predicts an operating empty weight (OEW) of 91,470 lb compared to the manufacturer's reported value of 88,175 lb. Although this represents only a 3.5% difference between predicted and actual weight, the FLOPS model was calibrated to the actual value by applying an overall reduction factor on empty weight. Calibration could not be performed for each individual component since actual weight data were not available at that level. A point on the payload-range diagram of reference 23 was used to calibrate the range performance of the FLOPS model. Assuming 31,000 lb of payload (155 passengers) and a takeoff gross weight of 156,000 lb, reported range capability for the MD-90-30 is approximately 2040 nm. The initial FLOPS-predicted range capability was significantly higher. There are a number of possible explanations for the range discrepancy, including using a different mission profile (cruise Mach, altitude, and reserve mission assumptions), differences in predicted and actual aerodynamic performance, and differences between the NASA engine model and actual engine fuel consumption characteristics. Without additional data in one of these areas, it is impossible to determine

the underlying cause. Because the FLOPS-predicted cruise aerodynamic efficiency did not seem optimistic and the cruise thrust specific fuel consumption (TSFC) seemed low compared to other engines of this class, range performance of the model was calibrated to the published value by adjusting the fuel flow rates of the V2525-D5 engine model. In reality, the range discrepancy is likely due to a combination of factors.

A series of modifications was necessary to progress from a MD-90-30-like FLOPS model to an appropriate advanced technology airframe model suitable for the open rotor engines. These steps are summarized in Figure 3 and described in more detail below.

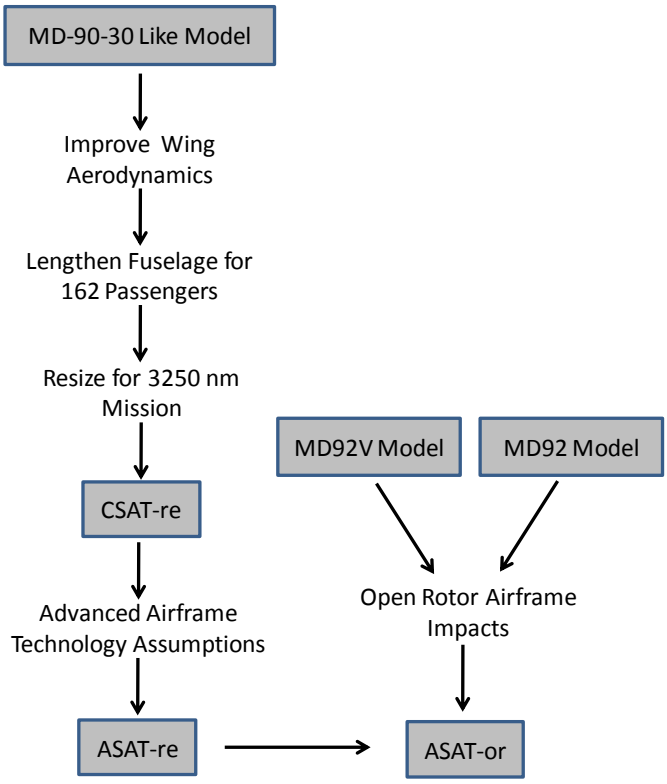


Figure 3. Process used to model advanced technology airframe suitable for open rotor propulsion.

Previous NASA studies of propulsion options for 737/A320 replacement designs (refs.17, 20) have used a Boeing 737-800-based airframe model and design mission. Although the MD-90-30-based model described above differs from the 737-800-based model in a number of respects, it was desired to at least have a consistent technology level and design mission for the baselines used in the two studies. Of critical importance in developing a consistent technology baseline is the level of airfoil design technology for the MD-90-30 wing. The MD-90-30 uses the same wing design as the older MD-80 series. This 1980s technology is not as advanced as the newer 737-800 wing (1998 entry-into-service). Although the exact difference in aerodynamic design technology between the 737-800 and MD-90-30 is not known in the public domain, there is some indication of the potential gap in aerodynamic efficiency provided by comparing the current 737 design to older models. One source indicates maximum M*(L/D) (Mach number times lift-to-drag ratio) of the 737-700 is 16% higher than the equivalent size, older generation 737-300 design (ref. 26). In order to advance the MD-90-30-like airframe model to late 1990s technology

levels, FLOPS aerodynamic factors were adjusted to provide a similar improvement in aerodynamic efficiency. The takeoff and landing aerodynamic performance was also modified. A model of the 737-800 low-speed performance was used as a rough approximation for the notional, updated version of the MD-90-30. Changes were made to the design mission to make it consistent with the prior studies. The study design mission (162 passengers, mixed class, 3250 nm) was selected to reflect performance enhancements projected for future advanced aircraft in this vehicle class. Although based on desired future capabilities, this design mission was also applied to the older technology baseline model to enable a consistent comparison with the advanced study vehicles. Since the MD-90-30 fuselage only accommodates 158 passengers in mixed class seating, the fuselage length was slightly increased to accommodate an additional row of seats. Wing area was increased to accommodate the higher gross weight needed to meet the design mission. The resulting airframe, referred to as CSAT-re (Current technology Single-Aisle Transport-rear engine), represents a model of the MD-90-30 updated to late 1990s entry-into-service technology levels and re-sized to perform the study design mission.

The Advanced Single-Aisle Transport-rear engine (ASAT-re) airframe model is a derivative of the CSAT-re model intended to be representative of a potential advanced technology single-aisle replacement aircraft. The primary airframe technology advancement assumed is extensive use of composite materials for the airframe structure. The composite construction is assumed to result in a 15% reduction in weight of the wing, fuselage, and empennage compared to the metal construction used for the CSAT-re airframe. This weight reduction represents an assumed benefit for future composite structures and is not necessarily a reflection of the benefit composite materials have provided to date. Other minor technology improvements include an increase in hydraulic pressure to 5000 psi, and a 1% reduction in drag associated with a variable camber trailing edge and general drag clean-up. The basic geometry parameters for the ASAT-re were not changed from the CSAT-re model.

The MD-90-30-based ASAT-re airframe layout is generally compatible with an open rotor propulsion system, and, in fact, open rotor propulsion was considered during the design of the MD-90 family. Reference 27 describes the design of both turbofan and open rotor configurations for the MD-90 family and details the modifications to the turbofan version that are necessary to accommodate an open rotor engine. To approximate the impact of those modifications, the MD-92 configurations described in reference 27 were examined and modeled in FLOPS. Reference 27 discusses several differences between the MD-92 (open rotor) and MD-92V (turbofan) airframe designs necessitated by the integration of the open rotor system. The fuselage weight is higher due to additional acoustic treatment for reduced interior noise, sonic fatigue treatment of the aft fuselage structure, and structural treatments to reduce vibrations. Hydraulic system weight is increased by an additional hydraulic system dedicated to the tail control surfaces. A center-of-gravity management system is needed to address stability and control issues introduced by the heavier aft engine weight and higher engine thrust line. The system-level impact of these differences, plus the higher weight of the open rotor engine, was a 4200 lb increase in empty weight. Since detailed weight increments were not provided in reference 27, this overall weight increase was allocated in an approximate manner to each of the above areas to develop a FLOPS model of the MD-92 from a MD-92V FLOPS model. The adjustments necessary to convert from the MD-92V (turbofan) to the MD-92 (open rotor) configuration were then applied to the ASAT-re model described above to develop the ASAT-or (Advanced Single-Aisle Transport-open rotor) model for use in the open rotor aircraft analysis. The nominal ASAT-or configuration is shown in Figure 4.

Figure 4. Basic Advanced Single-Aisle Transport configuration with rear-mounted open rotor engines (ASAT-or).

## 3.3 Noise Analysis

Prediction of FAR Part 36 certification noise (ref. 8) for open rotor propulsion is of critical importance in understanding the trades between lower fuel consumption and higher noise. Open rotor noise prediction is also an area with significant challenges. A number of counter-rotating open rotor source noise prediction methods were developed during NASA's previous studies of open rotors in the 1970s and 1980s. Perhaps the most promising of these methods are the semi-empirical codes described in references 28 and 29, which have recently been revived and validated on modern computing platforms. However, these methods predict only rotor-rotor discrete interaction tones and they are incapable of evaluating rotor broadband noise. They are also not capable of evaluating the noise of rotors having advanced, low-noise design features. Open rotor blades are now designed using modern, 3D aerodynamic analytical tools and advanced rotors will employ low-noise features, some of which have been made public and others that are still company-proprietary. Known rotor noise mitigation strategies include aeroacoustic blade shaping, blade pitch angle and rotational speed optimization, increased blade counts, low disk loading, rotor-rotor and pylon-rotor spacing optimization, aft rotor clipping, and pylon wake reduction (ref. 30). Because of the shortcomings of current rotor noise modeling capabilities, a system-level noise prediction method has been developed which uses noise data measured from scale model open rotor test articles.

### *3.3.1 Open Rotor Source Noise Modeling*

Tests of various open rotor designs have taken place in NASA Glenn's experimental facilities as part of an ongoing NASA-General Electric collaborative partnership (ref. 31). Low-speed aerodynamic and acoustic tests were conducted in the Glenn 9x15-ft Low Speed Wind Tunnel, and high-speed aerodynamic testing was conducted in the Glenn 8x6-ft tunnel. The open rotor acoustic data used for this assessment of certification noise was collected from one of General Electric's advanced "Gen-1" rotor blade sets.

The experimental setup is illustrated in Figure 5, showing a schematic of the open rotor rig and the linear microphone array. The microphone traverse array is located 60 inches from the centerline of the rotor model. Each tunnel acoustic "reading" consists of microphone-corrected, narrowband spectral density levels taken at 18 sideline microphone locations with frequencies ranging from zero to 100 kHz at frequency intervals of 12.2 Hz. Data were collected with the model operating at various shaft speeds and blade pitch angles. Both rotors were always operated at identical shaft speeds. Tests were also conducted

to estimate the facility's tare background noise levels with no power supplied to the open rotor test article and with no blades attached.

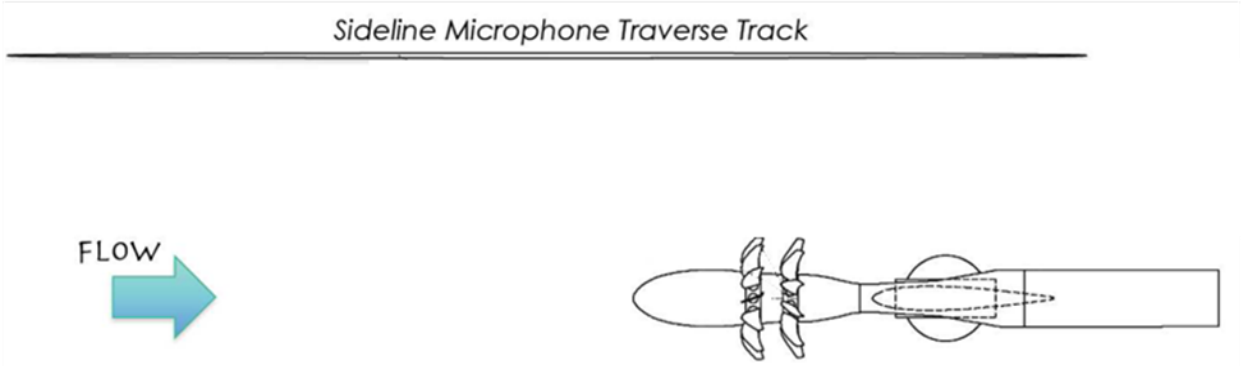


Figure 5. Open rotor test article and linear microphone array in the NASA Glenn 9x15-ft Low Speed Wind Tunnel. *(Diagram courtesy of Edmane Envia, NASA Glenn Research Center)*

The microphone-corrected spectral density levels were adjusted by the facility's data acquisition software to lossless, freefield conditions using an atmospheric attenuation model. The spectral density levels were further corrected for spherical spreading from the microphone's constant sideline distance to a 1-foot constant radius arc from a point originating on the rear rotor center of rotation. These data must be manipulated in several additional ways in order to properly predict certification noise for a full-scale aircraft. The spectra were modified further by applying the following corrections:

*1. Initial preparation*

The spectral density levels of the tare test were subtracted from each noise spectrum of interest in the powered tests over all frequencies. Next, the spectral densities were converted to sound pressure levels with a reference pressure of 20μPa. The geometric sideline microphone array angles ($\theta_G$) range from 18° to 140°, where the zero reference of $\theta_G$ is directly upstream. Emission yaw (polar) angles ($\theta_E$) were computed from the $\theta_G$ angles using the relation $\theta_E = \theta_G - \sin^{-1}[M_{Tunnel} \sin \theta_G]$, where the tunnel Mach number, $M_{Tunnel}$, in the experiments is 0.20. A small amount of data were collected for $M_{Tunnel} = 0.18$ and 0.22, but they were not used in this assessment.

*2. Conversion to static conditions*

The sound pressure levels were corrected for convection effects to static conditions by adding an amplitude correction of $10 \log_{10}[\, 1 - M_{Tunnel} \cos \theta_E \,]^{SME}$, where the source motion exponent (*SME*) was taken to be 2, for dipole emission. No Doppler adjustments were made to the frequency scale (i.e., $f_{Static} = f_{Tunnel}$), since the microphones were "traveling with" the source at the speed of the tunnel Mach number.

*3. Conversion to flight conditions*

The sound pressure levels were corrected to realistic takeoff and approach flight conditions by subtracting an amplitude convection correction of $10 \log_{10}[\, 1 - M_{Flight} \cos \theta_E \,]^{SME}$. The flight Mach number, $M_{Flight}$, is supplied via airplane trajectory calculations for approach and departure, and is discussed in later sections. The source motion exponent was again taken to be 2. A Doppler frequency shift ($f_{Flight} = f_{Static} / [\, 1 - M_{Flight} \cos \theta_E \,]$) was applied to the frequency scale. In addition, an amplitude adjustment of $10 \log_{10}[\, M_{Flight} / M_{Tunnel} \,]$ was made to account for observed increases in source levels with freestream Mach number. (This correction is based on experiments conducted by General Electric during the Advanced Turboprop Project.) Further, a source strength amplitude adjustment of $10 \log_{10}[(\rho_{Flight}/\rho_{Tunnel})^2 (c_{Flight}/c_{Tunnel})^4]$ was made to correct the spectra from tunnel conditions to flight

conditions, where $\rho_{Tunnel}$ and $c_{Tunnel}$ are the density and the speed of sound measured in the wind tunnel, respectively, and $\rho_{Flight}$ and $c_{Flight}$ are the density and the speed of sound at the simulated flight conditions. Standard acoustic day (ISA+18°F) values at altitudes predicted by the trajectory analysis were used for the flight conditions.

*4. Conversion to full scale*

The sound pressure levels were then corrected from model scale to full scale. Frequencies were shifted to lower values by dividing by the linear scale factor, $D_{Full\text{-}Scale}/D_{Rig}$, and amplitudes were adjusted by adding a correction of 20 $\log_{10}[\ D_{Full\text{-}Scale}/D_{Rig}\ ]$. The scale model test article front rotor diameter, $D_{Rig}$, was 2.4095 ft. $D_{Full\text{-}Scale}$ depends on the characteristics of the study engine (Section 4.1) and any engine thrust scaling performed to match the engine and airframe (Section 4.2). The final, sized front rotor diameter for the airplane in this study is 13.67 ft resulting in a linear scale factor ($D_{Full\text{-}Scale}/D_{Rig}$) of 5.673.

*5. Conversion to 1/3$^{rd}$ octave band spectra*

The frequency basis for FAA and ICAO aircraft noise certification is the traditional 1/3$^{rd}$ octave band center frequency spectrum, represented by 24 discrete sound pressure levels ranging from 50 Hz to 10,000 Hz. The acoustic energy contained in the intervals on either side of each center frequency (i.e., from $2^{-1/6}$ times the center frequency to $2^{1/6}$ times the center frequency) are summed to form each of the 24 standard 1/3$^{rd}$ octave band sound pressure levels. The band filter specified by Part 36 noise regulations is defined by the International Electrotechnical Commission (ref. 32).

Several of the processing steps discussed above are illustrated in Figure 6. For illustration purposes, spectra from a non-proprietary – but representative – rotor set were used. The sample spectrum was taken from a microphone reading in the forward quadrant. A one-foot-arc, lossless, narrowband, sound pressure level spectrum with facility noise removed is shown by the black line in Figure 6a. This spectrum has an emission yaw angle of 24° from the inlet, the tunnel Mach number was 0.20, and the open rotor test article was operating at a corrected shaft speed of 6300 rpm. Although noise measurements are available up to 100 kHz, only lower-frequency data are plotted. When flight condition scaling is applied (scaling to a flight Mach of 0.26 at 1000 ft is shown), the spectrum shifts to higher amplitudes and frequencies, as represented by the red line in the figure. Opposite shifting behavior occurs for spectra in the aft quadrant. Scaling from experimental tunnel conditions to appropriate, simulated flight conditions can result in changes of several decibels in the fore or aft quadrants and is thus an important processing step. When the scale factors are applied to convert from model scale to full scale, the spectrum shifts to much higher amplitudes and lower frequencies represented by the blue lines in Figure 6a and Figure 6b. At one-fifth scale, the inaudible sound pressure levels measured at frequencies of about 50 kHz are shifted to the audible, regulated range used to estimate noise certification levels.

The 1/3$^{rd}$ octave band sound pressure levels are plotted in Figure 6b. The fundamental blade passage frequency tones for the front and aft rotors are labeled “1f” and “1a” in the figure, respectively. Since the front rotor has 12 blades and the aft rotor has only 10 blades in this particular design, the fundamental tone of the front rotor is always at a higher frequency than the fundamental tone of the aft rotor. Unequal blade counts distribute the tones over a wider frequency range and help reduce noise. Several higher-order rotor-rotor discrete interaction tones are also noted in the figure. Seldom do any of the interaction tones above the 2f+2a tone contribute significantly to the overall sound pressure level. The reasoning behind the frequency “coarsening” from the narrowband to the 1/3$^{rd}$ octave band is that the resulting spectra become much easier to manipulate and store. However, many of the rotor-rotor interaction tones lie within a single frequency interval, such that a single 1/3$^{rd}$ octave band sound pressure level may incorporate two (or more) tones. This is particularly true at higher frequencies since the scale is logarithmic.

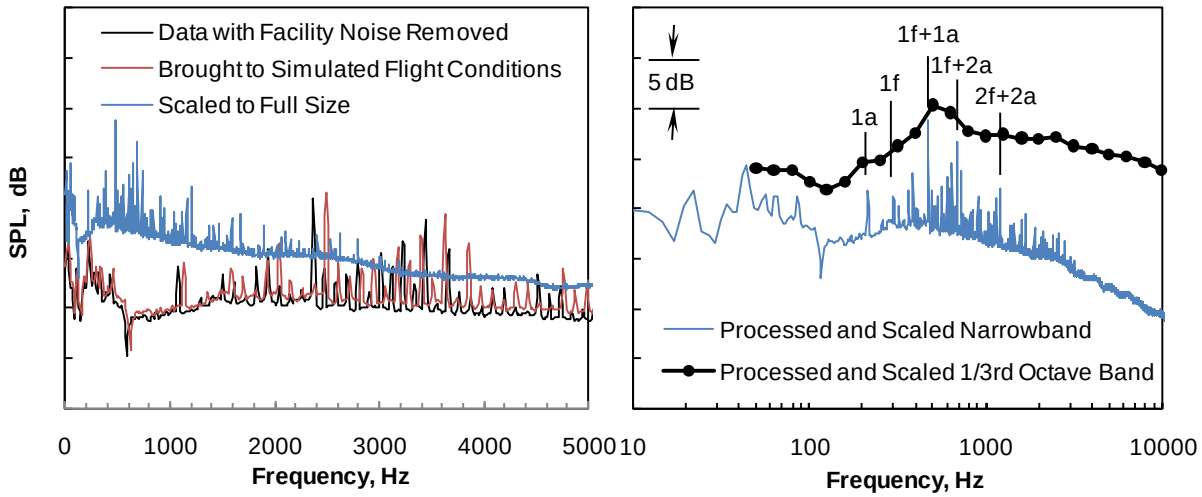


a) Conversion to full scale.

b) Conversion to 1/3rd octave band.

Figure 6. Sample open rotor narrowband spectrum conversions.
($M_{Tunnel}$ =0.2, $\theta_E$ =24°, corrected shaft speed=6300 rpm)

### *3.3.2 System-Level Noise Predictions*

The Aircraft Noise Prediction Program (ANOPP) Release Level 30 (refs. 33, 34) is a systems-level code used in this study to compute certification noise for the open rotor airplane. The center frequency basis for ANOPP is the 1/3rd octave band. The scaled 1/3rd octave band open rotor spectra described above were fed into ANOPP via its Acoustics Data Module (ACD). ACD is an ANOPP utility that allows user-supplied spectra to be fed into a certification simulation in lieu of using ANOPP's own, built-in, source noise prediction modules (ref. 35). Core, jet, and airframe noise sources were modeled using the ANOPP methods described in references 36, 37, and 38, respectively. Using an assumption of acoustic superposition, the freefield, lossless spectra for all of the noise sources were analytically summed in the vicinity of the aircraft. Real noise sources are, of course, complex, distributed signals that are affected by other acoustic sources, aircraft external surfaces, and the environment. No attempt was made to adjust the component spectra for acoustic near-field phenomena such as source interactions, reflections, refraction, diffraction, or other effects.

An airplane model with appropriate low-speed aerodynamics, weight, and propulsion performance data is necessary to model the takeoff and approach trajectories needed for aircraft certification predictions. The airplane was modeled using the FLOPS computer program as described in Section 3.2. FLOPS computes detailed, low-speed takeoff and landing profiles using a built-in, time-stepping trajectory analysis module. A takeoff and landing analysis was performed with FLOPS for a sea level field, with zero gradient, at standard acoustic day (ISA+18°F) conditions using the vehicle's low-speed aerodynamics and the open rotor thrust data. Compliance with the airworthiness requirements described in Parts 36 and 25 of the Federal Aviation Regulations (references 8 and 39, respectively) was observed. For takeoff, maximum takeoff gross weight was assumed and the flaps were set at detent 5. The takeoff procedures were as follows:

1. Brake release at maximum Sea Level, Static (SLS) rated thrust
2. Ground run

3. Rotate such that liftoff velocity is at least 110% of the minimum unstick velocity with all engines operating, or 105% of minimum unstick velocity with one engine inoperative
4. Climb to the 35 ft obstacle at maximum thrust
5. Raise gear
6. Climb at constant calibrated airspeed at maximum thrust
7. From 16,000 ft to 17,000 ft from brake release, reduce thrust to the minimum allowable cutback value (such that climb gradient is zero with one engine inoperative, or 4% with all engines operating)
8. Climb at constant calibrated airspeed at cutback thrust
9. At 30,000 ft from brake release, increase thrust to "power-up" level
10. Climb at constant calibrated airspeed at power-up thrust

For approach, a 3° glide slope was followed, the maximum landing weight was assumed, and the flaps were set at detent 40 with leading edge slats and landing gear deployed.

Vector geometry analyses for the airplane relative to the three certification microphone measurement locations – shown in Figure 7 – were performed within ANOPP as functions of source time. The spectra were then propagated to the three certification observers on the ground in accordance with the specifications for certification measurements.

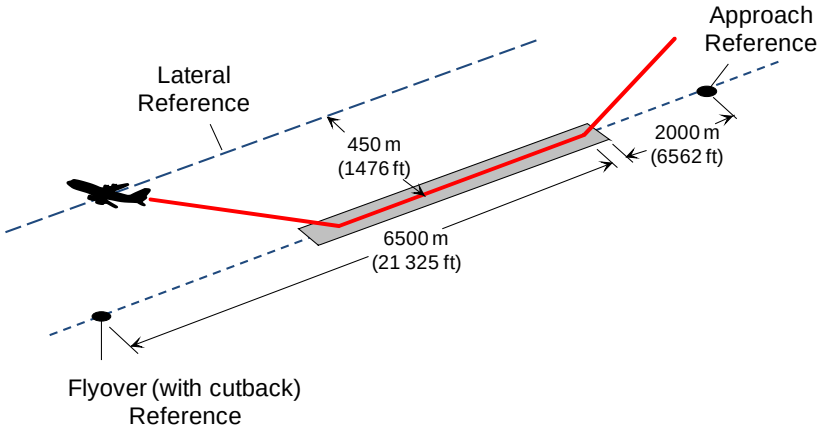


Figure 7. Noise observer arrangement relative to takeoff and landing aircraft trajectories.

Noise propagation effects accounted for included spherical spreading, Doppler shift and convective amplification, atmospheric absorption (ref. 40) and variable impedance effects within a layered atmosphere, ground reflections (ref. 41) based on data for grass-covered ground (ref. 42), and lateral attenuation (ref. 43). To account for incoherently-radiating twin engines, 3dB were added to the propulsion noise sources. More complex propagation phenomena such as scattering, weather effects, and terrain were not modeled.

From the propagated spectra, ANOPP computes several noise metrics of interest as functions of observer time. The Effective Perceived Noise Level (EPNL) certification noise metric is computed from the noise-time history at each observer as prescribed in reference 8.

### *3.3.3 Special Considerations for Open Rotor Aircraft*

In a propeller-driven aircraft noise certification test (or a simulation of one), the tone-rich acoustic spectra observed by the microphones fluctuate significantly when tones move from one frequency interval

into another as the aircraft-observer geometry changes in flight, and convective amplification and Doppler effects come into play. This leads to irregular tone-corrected, perceived noise level (PNLT) vs. time histories as the airplane traverses a path relative to its certification observers. These irregularities are enhanced when ground reflections are present – causing ground nulls and pseudotones – particularly at frequencies under about 800 Hz, where ground effects are most efficient and where many propeller tones exist (as can be seen in Figure 6b). This effect is observed for current large turboprops in the transport category and may be observed one day for open rotor airplanes.

A special computational procedure unique to transport-category propeller aircraft was developed to handle the tone correction penalties from spectra that are rich in both real rotor tones and fictitious pseudotones. If tones are propagated to an observer, regulations (ref. 44) permit tone correction penalties resulting from them to be ignored provided the tones can be shown to be unrelated to engine source noise, since they may be artifacts of ground reflections. When PNLTs are analytically computed in this study, two ANOPP runs are made. In the first run, the sources are analytically flown past the observers, the ground reflection calculations are turned off, and the tone correction penalties at half-second intervals are saved. In the second run, the sources are again flown past the observer, the ground reflection calculations are turned on, and the PNL metric is computed at half-second intervals. The tone correction penalties from the first run are added to the PNLs from the second run, and the result is integrated to form the certification metric, the EPNL. Thus, this process is effective at excluding pseudotones from the tone correction calculations. This procedure is believed to be consistent with the regulations found in Ref. 44, but it has not been verified with regulatory authorities.

Another issue related to the tone correction penalty is the location of the lateral observer. Propeller tones were reason that the lateral observer location for large, transport-category, propeller-driven commuter transports was changed in 2002 from the 450 m (1476 ft) lateral sideline to a flyover point directly under the flight path where the airplane has reached an altitude of 650 m (2133 ft). (See Section B36.3(a)(2) of Part 36 (ref. 8) beginning in 2003.) The lateral observer relocation was permitted because of the difficulty inherent in determining the location of peak noise on the lateral sideline for turboprop aircraft due to the large number of ground nulls and pseudotones caused by ground reflections. With the observer located on the extended runway centerline, ground effects are less efficient because the airplane is flying directly overhead and the angles that the source subtends with the horizon are greater. In this study, however, the lateral observer location for the NASA notional open rotor airplane is assumed to remain on the 450 m lateral sideline (as required for jet aircraft in Section B36.3(a)(1) of Part 36, ref. 8). This is because an open rotor vehicle will likely be larger than commuter turboprops, and it will naturally be compared to (and compete with) contemporary, large, single-aisle jet aircraft. At this writing, however, placement of the lateral observer remains an open issue for large, open rotor transports. With lateral attenuation modeling included, the peak EPNL along the lateral sideline occurs across from the point where the airplane reaches an altitude of about 900 ft above field elevation.

The approach and flyover observers are located on the extended runway centerline as prescribed by reference 8, with the approach observer located 2000 m (6562 ft) from the runway threshold (or, assuming a 50 ft landing obstacle and a 3 degree glide slope, 2291 m (7518 ft) from the touchdown point), and the flyover observer located 6500 m (21,325 ft) from brake release. See Figure 7 for a sketch of these locations.

### *3.3.4 Establishing Reference System Noise Levels*

Seventy-two acoustic readings collected from the NASA Glenn 9x15-ft Low Speed Wind Tunnel were used in establishing reference system noise levels. These readings, made during May 2010, had an

isolated nacelle (i.e., no pylon or simulated fuselage was used) and a muffler system to effectively suppress the noise of the drive rig. All 72 readings were made at a Mach number of 0.20. Data were collected at a variety of blade pitch angles and shaft speeds. Front rotor advance ratios (varied by changing the rotor shaft speeds) ranged from 0.82 to 1.48.

The acoustic readings were scaled and analytically flown past the observers as described in earlier sections and EPNLs were computed for each of them. An example of this procedure is shown in Figure 8 for the flyover observer. In this case, the open rotor is operating at a corrected tip speed of 655 ft/s with a front blade pitch angle of 36.8°. The linear scale factor, flight Mach number, and altitude used to scale the spectra are 5.673, 0.269 and 2050 ft, respectively. The PNLTs are plotted against the observer time from brake release at half-second intervals (left), and against the polar emission angle (right). The EPNL (81.0 EPNdB in this case) is computed by integrating the PNLT vs. time curve using only the points within 10 PNdB of the maximum. The jet, core, and airframe noise sources also contribute to the overall levels. Jet noise, however, is virtually negligible in all cases due to the low core jet velocities exiting the power turbine. Airframe and core sources contribute only at approach, when rotor noise levels are relatively low.

In the tunnel, microphone readings were taken from polar geometric angles ranging from 18° to 140°. With the tunnel operating at Mach 0.20, the polar emission angles range from 14° to just 133°. Unfortunately, when the sources fly past an observer, noise remains within 10 PNdB of the maximum until the source recedes beyond 150°. There is a region in the "10 PNdB-down" area where the emission angles are greater than the aft most microphone reading of 133°. In this region, the aft most microphone spectrum is simply repeated as the aircraft recedes until spherical spreading diminishes its level.

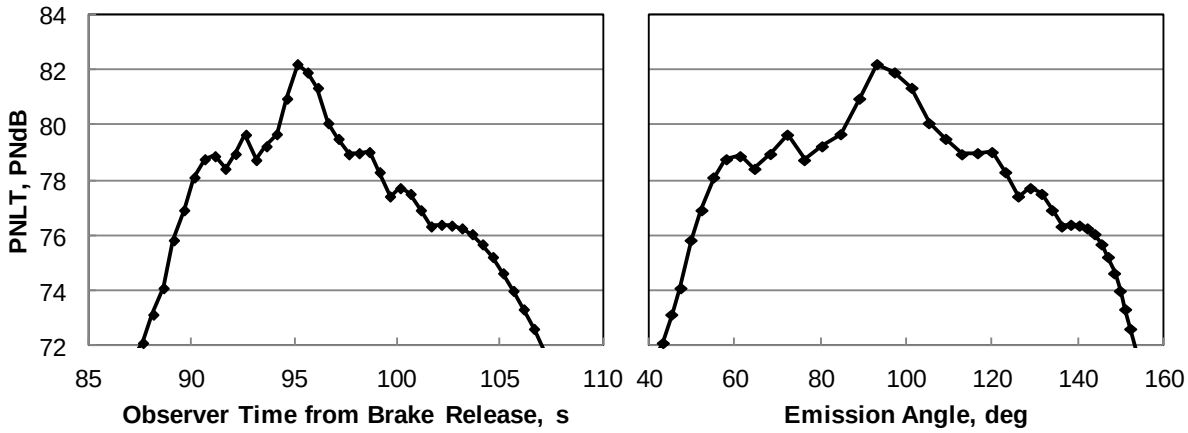


Figure 8. Example flyover observer PNLT noise histories for a case with rotor corrected tip speed of 655 ft/s.

The set of 72 EPNLs correlate very well with several independent variables such as rotor thrust, tip speed, and blade pitch angle. To obtain the reference system EPNL for each of the three certification observers, the characteristics of the airplane as it flies past each observer must be matched against the EPNL dataset. In other words, the EPNL for each observer is selected based on the thrust demand and flight conditions of the airplane. The thrust, altitude, airspeed, and angle of attack are known via the takeoff and approach trajectory calculations described in Section 3.3.2 and shown later in Section 4.3.1. This thrust-noise matching procedure requires that the thrust levels measured by the wind tunnel open rotor propulsion rig be scaled to the thrust that an actual full-size open rotor propulsion system would produce in flight. Thrust scaling is a simple proposition for a propeller that maintains geometric and aerodynamic similarity throughout the takeoff and landing flight regime. However, in practice, variable-

pitch propellers operate in flight conditions that are decidedly not similar to the tests conducted in the tunnel. For practical engine operational and performance reasons, the rotor tangential tip speed (and shaft speed) is held constant. Rotor blade pitch angle is varied as flight conditions change to provide the thrust required. As the airspeed increases from zero at brake release to climbout velocities of well over 150 kts, the advance ratio increases as well. Blade pitch angles must increase with airspeed to maintain peak efficiency. With a constant-speed propeller, scaling thrusts from the wind tunnel Mach number (0.20) to the flight Mach number (often in excess of 0.26) is required.

No theoretical scaling approach is perfect in non-similitude cases. Ideally, if there were sufficient wind tunnel data collected at a variety of low-speed flight Mach numbers, a simple empirical thrust correction factor model could be developed. However, nearly all of the open rotor data were collected at a wind tunnel Mach number of 0.20. Therefore, instead, a simple thrust correction multiplier is required that performs reasonably well for minor excursions in flight conditions in the takeoff regime. This correction is discussed in greater detail in the Appendix. The correction adjusts the rotor thrusts measured in the tunnel to the appropriate flight conditions by applying multipliers of the density ratio, diameter ratio, and a factor that accounts for the inlet ram drag and core nozzle thrust of the engine. The results of the thrust-noise matching procedure will be presented in Section 4.3.2.

### *3.3.5 System Corrections to Reference Noise Levels*

Several important system-level adjustments must be made to each of the reference EPNLs. Since the reference EPNLs represent the noise signature of an isolated open rotor nacelle in a uniform flowfield with steady loading, corrections are required to account for the effect of the rotor inflow angle, the presence of an upstream engine pylon, and pylon wake mitigation strategies envisioned by NASA and General Electric. Other system-level effects not accounted for in the current analysis include fuselage and tail shielding effects on the lateral observer, other fuselage effects, T-tail reflections, and flowfield effects due to rotor rotation direction.

The open rotor wind tunnel model was tested at rotor inflow angles of 0°, 3°, and 8° by angling the rig into the freestream flow. Rotor noise was found to be a strong function of rotor inflow angle due to the unsteady aerodynamic loading effects on the rotor blades. To use the wind tunnel data collected at nonzero angles to account for inflow effects, the rotor inflow angle, $\alpha_{Inflow}$, must first be related to the angle of attack of the airplane, $\alpha$, (known from the trajectory analysis). A vortex-lattice aerodynamic analysis was performed to estimate the angularity of the flow at the rotor location. For this linear analysis, $\alpha_{Inflow}$ may be expressed as:

$$\alpha_{Inflow} = \alpha_{Cant} - \varepsilon_0 + \alpha\left[1 - d\varepsilon / d\alpha\right]$$

where $\alpha_{Cant}$ is the propulsion system mounting cant angle (relative to the aircraft zero angle of attack line), $\varepsilon_0$ is the downwash angle at the rotor when $\alpha = 0$, and $d\varepsilon/d\alpha$ is the variation of downwash with airplane angle of attack. The parameters $\varepsilon_0$ and $d\varepsilon/d\alpha$ are functions of the wing configuration (i.e., they vary with the amount of flap and slat extension).

To set the cant angle, the vehicle was first analyzed in a clean configuration at cruise flight conditions and the downwash angle into the rotor face was computed. The cant angle, $\alpha_{Cant}$, was then set to 2° (nose-up) such that the rotor inflow angle is approximately zero at the cruise flight condition. The vehicle then was analyzed in departure (partial flaps deployed) and approach (full flaps and slats deployed) configurations. On departure, $\varepsilon_0$ and $d\varepsilon/d\alpha$ were found to be 2.34° and 0.336, respectively. On approach, $\varepsilon_0$ and $d\varepsilon/d\alpha$ were found to be 5.19° and 0.349, respectively. Using the $\alpha$ computed during the aircraft

trajectory analysis, the approximate rotor inflow angle was computed at each observer and an appropriate inflow angle noise penalty assigned to each EPNL.

The increase in rotor noise due to the pylon wake impinging on the front rotor was estimated by an examination of data from testing of General Electric's historical baseline rotor design in the presence of an upstream engine pylon. Only eight readings were taken with the pylon in place. Four readings were made at zero inflow angle, and two readings were made at inflow angles of 3° and 8°. With this limited amount of data available, it was observed that the greatest pylon noise impact occurred at zero inflow angle and at low thrust levels. There was virtually no distinguishable impact at the 8° inflow angle. Some of the pylon noise impact can be reduced by applying pylon wake mitigation technologies under consideration by NASA and General Electric. To account for the presence of a pylon with successful implementation of pylon wake mitigation strategies, penalties of 0.6, 0.3, and 0.6 EPNdB were assigned to the approach, lateral, and flyover EPNLs, respectively.

# 4.0 Analysis Results

## 4.1 Engine Design

General characteristics of the NASA advanced open rotor engine are shown in Table 1, additional details are provided in reference 19. Also shown for comparison are the characteristics of one of NASA's advanced geared turbofans from reference 20 and NASA's model of the V2525-D5 turbofan, which powers the MD-90-30 aircraft used as the starting point for the open rotor aircraft concept. Four different geared turbofan designs were developed in reference 20. The geared turbofan selected for comparison here is the fan pressure ratio (FPR) 1.5 engine, which resulted in the lowest mission fuel consumption in that study. The open rotor engine was designed for 5,000 lb of thrust at top-of-climb (TOC) conditions (M=0.78, 35,000 ft) and 19,000 lb of thrust at hot day, rolling takeoff conditions (M=0.25, SL). The open rotor engine was initially designed for 17,800 lb of thrust at hot day, rolling takeoff conditions. However, the operating temperatures at cruise for the resulting engine were too high. As a result, the final open rotor engine is "oversized" for takeoff. This excess thrust can be used for improved takeoff performance, or the engine could be "de-rated" for takeoff which would improve engine life. The geared turbofan design conditions are slightly different: 5,000 lb at M=0.8, 35,000 ft and 17,500 lb at the hot day, rolling takeoff condition. The TOC thrust and TSFC values in Table 1 are given for the M=0.78 open rotor TOC condition for a consistent comparison. The advanced geared turbofan and open rotor engines are shown graphically in Figure 9.

The expected efficiency benefits of the advanced open rotor architecture are clearly evident in Table 1. At the M=0.78, 35,000 ft top-of-climb point, the open rotor engine TSFC of 0.428 lb/(lb·h) is approximately 13% lower than for the FPR=1.5 geared turbofan (0.494 lb/(lb·h)) and 30% lower than for NASA's V2525-like model (0.610 lb/(lb·h)). The reduction in TSFC is even greater for the SLS and rolling takeoff conditions. At SLS conditions, the open rotor TSFC of 0.158 lb/(lb·h) is 39% lower than for the advanced geared turbofan and 54% lower than for the V2525-like engine. Similar reductions in TSFC are obtained at rolling takeoff conditions. These improvements in TSFC at SLS and rolling takeoff should lead to much lower fuel consumption and emissions in the airport terminal area. Landing-Takeoff (LTO) $NO_X$ characteristics are presented in Table 1 in terms of the regulated parameter, $D_p/F_{oo}$, where $D_p$ is the grams of $NO_X$ emitted over a standard LTO cycle (by a single, uninstalled engine) and $F_{oo}$ is the rated output at SLS conditions in kilonewtons. This parameter is defined by ICAO and used in FAR Part 34 for engine certification (ref. 45). $D_p/F_{oo}$ for the open rotor engine is 12.15 g/kN, 78% less than for the V2525-D5. The reduction in LTO $NO_X$ emissions compared to the V2525 engine comes from a combination of lower $NO_X$ emission indices (EIs) due primarily to an advanced low $NO_X$ combustor and

lower fuel flow (higher efficiency) at the ICAO-defined LTO operating points. The advanced geared turbofan engine has the same advanced combustor as the open rotor, and similar $NO_X$ EIs. However, the significantly lower fuel flow of the open rotor engine leads to a 45% reduction in $D_p/F_{oo}$ compared to the advanced geared turbofan. The estimated $NO_X$ $D_p/F_{oo}$ of 12.15 g/kN for the open rotor engine is 79% below the current ICAO regulatory limit, established at the sixth meeting of the Committee on Aviation Environmental Protection.

The reduction in TSFC and LTO $NO_X$ does not come without penalty. Despite the use of advanced materials in the open rotor engine, the thrust-to-weight ratio (T/W) of the open rotor engine is actually lower than for the older technology V2525-D5 turbofan. The T/W of the open rotor engine at top-of-climb is 0.54, 25% lower than for the V2525-like model and 28% lower than for the advanced geared turbofan. At the aircraft system level, the benefit of the large TSFC reduction is offset somewhat by the lower engine thrust-to-weight, as well as the additional airframe weight associated with accommodating open rotor propulsion.

Table 1. General Engine Characteristics

| | V2525 Turbofan Model | Advanced Geared Turbofan (FPR=1.5) | Geared Open Rotor |
|---|---|---|---|
| **Overall Length, ft** | 18.3 | 15.8 | 23.2 |
| **Nacelle Diameter, ft** | 8.0 | 7.6 | 5.6 |
| **Rotor Diameter, ft (front / rear)** | N/A | N/A | 13.8 / 13.1 |
| **Engine+Nacelle Wt., lb** | 7900 | 6626 | 9218 |
| **Thrust** | | | |
| Sea Level, Static | 25,000 | 23,370 | 27,260 |
| Rolling Takeoff (M=0.25; SL) | 24,400 | 17,500 | 19,000 |
| Top-of-Climb (M=0.78; 35kft) | 5,685 | 4,960 | 5,000 |
| **TSFC, lb/(lb·h)** | | | |
| Sea Level, Static | 0.344 | 0.257 | 0.158 |
| Rolling Takeoff (M=0.25; SL) | 0.480 | 0.352 | 0.229 |
| Top-of-Climb (M=0.78; 35kft) | 0.610 | 0.494 | 0.428 |
| **Thrust-to-Weight** | | | |
| Sea Level, Static | 3.16 | 3.53 | 2.96 |
| Rolling Takeoff (M=0.25; SL) | 3.09 | 2.64 | 2.06 |
| Top-of-Climb (M=0.78; 35kft) | 0.72 | 0.75 | 0.54 |
| **LTO Fuel Flow (kg/s)** | | | |
| Take-off | 1.053 | 0.728 | 0.521 |
| Climb Out | 0.880 | 0.602 | 0.427 |
| Approach | 0.319 | 0.192 | 0.139 |
| Idle | 0.128 | 0.067 | 0.046 |
| **LTO $NO_X$ Emission Index (g/kg)** | | | |
| Take-off | 26.5 | 16.5 | 14.0 |
| Climb Out | 22.3 | 10.7 | 9.0 |
| Approach | 8.9 | 9.0 | 9.0 |
| Idle | 4.7 | 5.0 | 5.0 |
| **LTO $NO_X$, $D_p/F_{oo}$ (g/kN)** | 56.20 | 22.00 | 12.15 |

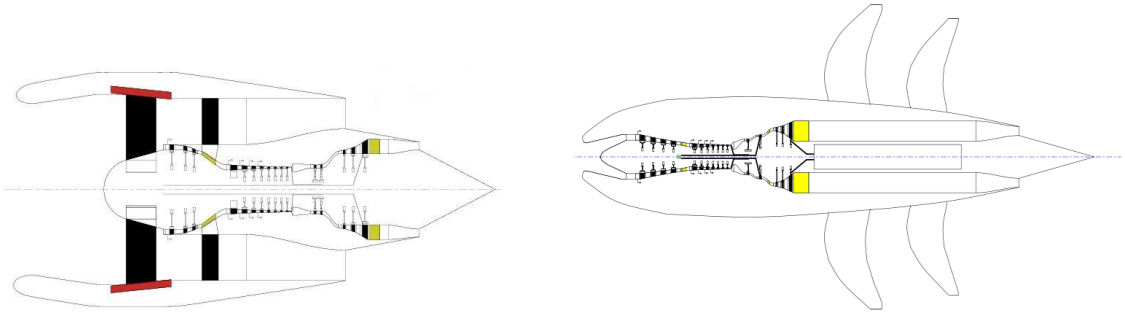

a) Geared turbofan. b) Geared open rotor.

Figure 9. Advanced engine architectures (not to scale).

## 4.2 Aircraft Sizing and Performance

The open rotor engine described above was combined with NASA's ASAT-or airframe model to determine overall aircraft performance for the open rotor configuration. The advanced FPR=1.5 geared turbofan was also combined with the ASAT-re airframe model for a comparison configuration. Each configuration was sized to meet the same mission requirements: 162 passengers (32,400 lb), 3250 nm range, cruise Mach of 0.78. Wing area and engine thrust were optimized to meet the mission requirements with minimum gross weight, subject to constraints such as takeoff field length, second segment climb gradient, approach speed, landing field length, missed approach climb gradient, rate-of-climb at initial cruise altitude, and wing fuel volume. The characteristics of the resulting vehicles for each of the advanced engines are summarized in Table 2. Also included for comparison are results for the CSAT-re baseline technology airframe combined with the NASA V2525-D5-like engine model and sized for the same mission requirements. This vehicle is referred to as the "1990s Technology Baseline." Weight, fuel consumption, and $NO_X$ emission results are also presented graphically in Figure 10.

Table 2. Aircraft Sizing Results

| | ***1990s Tech. Baseline*** | **ASAT-re FPR=1.5** | **ASAT-or Geared OR** |
|---|---|---|---|
| OEW, lb | *94,450* | 79,650 | 87,800 |
| Mission Fuel, lb | *49,160* | 35,800 | 31,050 |
| Payload Weight, lb | *32,400* | 32,400 | 32,400 |
| Ramp Weight, lb | *176,000* | 147,850 | 151,270 |
| Wing Area, $ft^2$ | *1530* | 1240 | 1250 |
| Wing Loading, $lb/ft^2$ | *115* | 119 | 121 |
| Thrust (SLS), lb | *25,190* | 23,075 | 26,900 |
| Thrust-to-Weight (takeoff) | *0.286* | 0.312 | 0.356 |
| Takeoff field length, ft | *7000* | 7000 | 6260 |
| Landing field length, ft | *5800* | 5940 | 6010 |
| ~Cruise Range Factor, nm (velocity*(L/D)/TSFC) | *12,670* | 14,730 | 17,170 |
| Block Fuel, lb | *41,550* | 30,390 | 26,710 |
| Total $NO_X$, lb | *292* | 205 | 216 |
| LTO $NO_X$, lb per cycle | *27.8* | 9.9 | 6.4 |

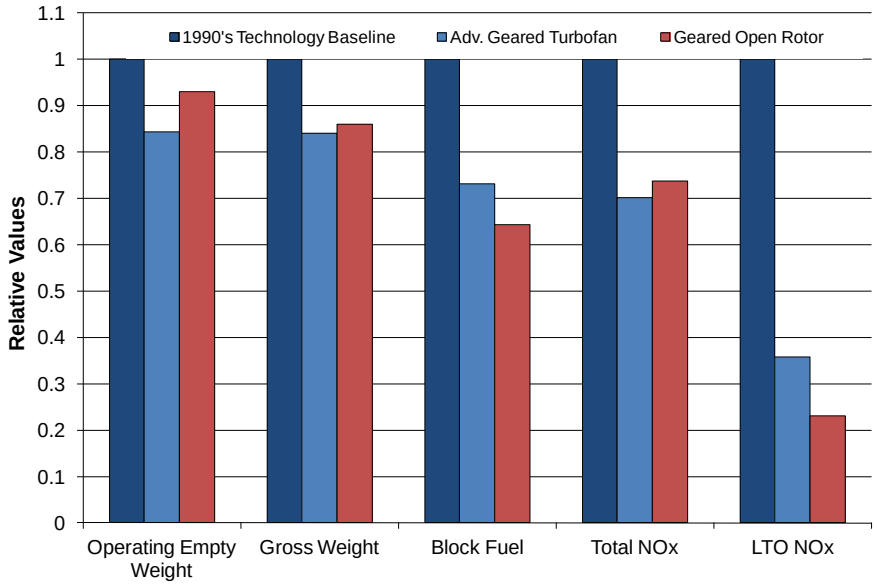


Figure 10. Advanced vehicle weight, fuel, and emissions relative to 1990s technology baseline.

As evident in Table 2 and Figure 10, both the advanced geared turbofan and advanced open rotor configurations have large weight, fuel consumption, and $NO_X$ emissions benefits over the 1990s technology baseline configuration. Empty weight reductions for the advanced configurations are relatively modest, mainly reflecting the benefits of a composite airframe and the cascading effects of a reduction in fuel weight. For the advanced open rotor vehicle, this benefit is offset to some extent by the much heavier engine. As a result, the open rotor configuration has higher empty weight and gross weight than the advanced geared turbofan configuration. Relative to the 1990s baseline, fuel consumption benefits are ~27% for the advanced geared turbofan and ~36% for the advanced open rotor. These reductions are from a combination of advanced airframe technology, advanced engine core technology, and advanced engine architectures. The reductions in total $NO_X$ emissions compared to the baseline are around 30% for both advanced configurations. Even though the open rotor configuration burns less fuel than the geared turbofan configuration, it emits more total $NO_X$. The average cruise $NO_X$ EI is 5.1 for the advanced turbofan and 7.2 for the open rotor engine. Both engines have advanced low $NO_X$ combustors, but the combustion temperature is higher in the open rotor engine. LTO $NO_X$ emissions are greatly reduced for both advanced configurations. The LTO $NO_X$ emissions presented in Table 2 and Figure 10 are the estimated total $NO_X$ emissions produced during the landing-takeoff cycle. This value is derived by multiplying the ICAO $D_p/F_{oo}$ parameter by the total engine thrust. LTO $NO_X$ emitted by the open rotor advanced configuration is less than one-fourth of the amount emitted by the baseline. The advanced geared turbofan configuration has extremely low LTO $NO_X$ emissions as well, slightly more than one-third of the baseline value.

To determine the true fuel consumption benefits of the open rotor architecture alone, comparison needs to be made to an equivalent technology turbofan configuration. The block fuel consumption of the advanced geared turbofan and advanced open rotor configurations are compared in Figure 11 for missions of various distances (all with 32,400 lb of payload). At the design point of 3250 nm, the open rotor architecture reduces fuel consumption 12% compared to an equivalent technology geared turbofan. This fuel consumption benefit is much less than the 20-25% reduction benefit often found in studies of the 1980s. One reason for this lower benefit is the high cruise Mach number that is being pursued with modern open rotor engines. Modern blade design techniques have reduced the loss in efficiency associated with high Mach rotors, but the advantage of open rotors over ducted turbofans is still greater at the lower Mach numbers which were usually assumed in the earlier studies. A second reason for the smaller benefit in the current study is the ultra-high bypass ratio of the comparison geared turbofan. The efficiency benefits of the higher effective bypass ratio of the open rotor are less when the bypass ratio of the ducted turbofan engine is ~14 as in the current study instead of ~6 as in past studies. Finally, most of the past studies were focused on the benefits of open rotor propulsion on short range missions. As shown in Figure 11, the fuel consumption benefits of the open rotor engine increase at lower ranges. At a range of 500 nm, the reduction in fuel consumption for the open rotor grows to 18%. Table 3 compares the fuel consumption by mission segment for the open rotor and geared turbofan configurations on the 500 nm and 3250 nm missions. The fuel consumption benefits of the open rotor are the lowest during cruise, ~10%, whereas fuel consumption reduction approaches 30% during other mission segments. For the short range mission, where cruise fuel is only about one-third of the total fuel use, the overall combined benefit is an 18% reduction in fuel use. (Note this particular mission profile is flown with optimum cruise altitude, leading to a climb mission segment that is almost as long as the cruise segment.) For the 3250 nm mission, where cruise fuel accounts for over 85% of the total fuel use, the open rotor engine overall benefit drops to 12%.

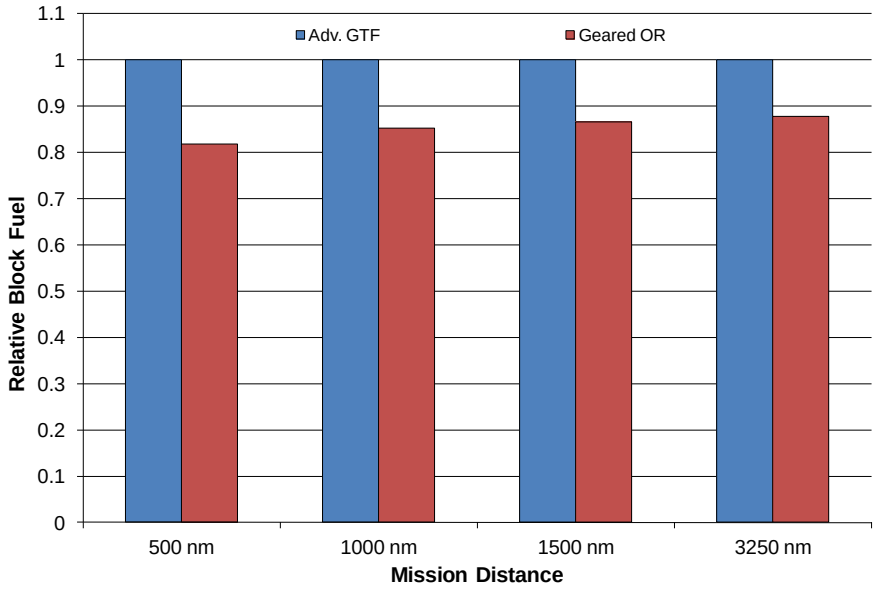


Figure 11. Block fuel comparison for advanced configurations.

Table 3. Fuel Consumption (lb) by Mission Segment

| | 500 nm Mission | | 3250 nm Mission | |
|---|---|---|---|---|
| Mission Segment | Adv. Geared TF | Adv. Open Rotor | Adv. Geared TF | Adv. Open Rotor |
| Taxi Out | 142 | 102 (-28%) | 142 | 102 (-28%) |
| Takeoff | 395 | 284 (-28%) | 395 | 284 (-28%) |
| Climb | 2602 | 2045 (-21%) | 2983 | 2353 (-21%) |
| Cruise | 1786 | 1643 (-8%) | 26,366 | 23,601 (-10%) |
| Descent | 304 | 224 (-26%) | 304 | 223 (-27%) |
| Approach | 126 | 91 (-28%) | 126 | 91 (-28%) |
| Taxi In | 79 | 57 (-28%) | 79 | 57 (-28%) |
| **TOTAL** | 5,435 | 4,444 (-18%) | 30,396 | 26,709 (-12%) |

## 4.3 Certification Noise

### *4.3.1 Trajectory Analysis*

Takeoff and approach trajectories and engine throttle settings must be modeled properly to correctly compute certification noise. An open rotor engine's thrust characteristics differ from the performance of turbofans, and a trajectory calculation is necessary to capture these effects. This is in contrast to the simplified certification noise estimates often made during the conceptual phase of aircraft design, where fixed trajectories and throttle settings are assumed based on previously-collected data from other representative aircraft. Trajectory data computed for the open rotor airplane are shown in Figures 12 and 13. Aircraft parameters (altitude above field elevation (AFE), airspeed, Mach number, and angle of attack) are shown in Figure 12 and engine parameters (net thrust per engine, thrust fraction, advance ratio,

and blade pitch angle) are shown in Figure 13. The trajectory is presented as a single operation with both takeoff and landing data shown simultaneously. For presentation purposes, the touchdown point on landing is coincident with the point of brake release on takeoff. The triangular markers on each plot denote the three noise certification measurement locations. The lateral observer is located on the lateral sideline at the distance from brake release where peak lateral noise is predicted.

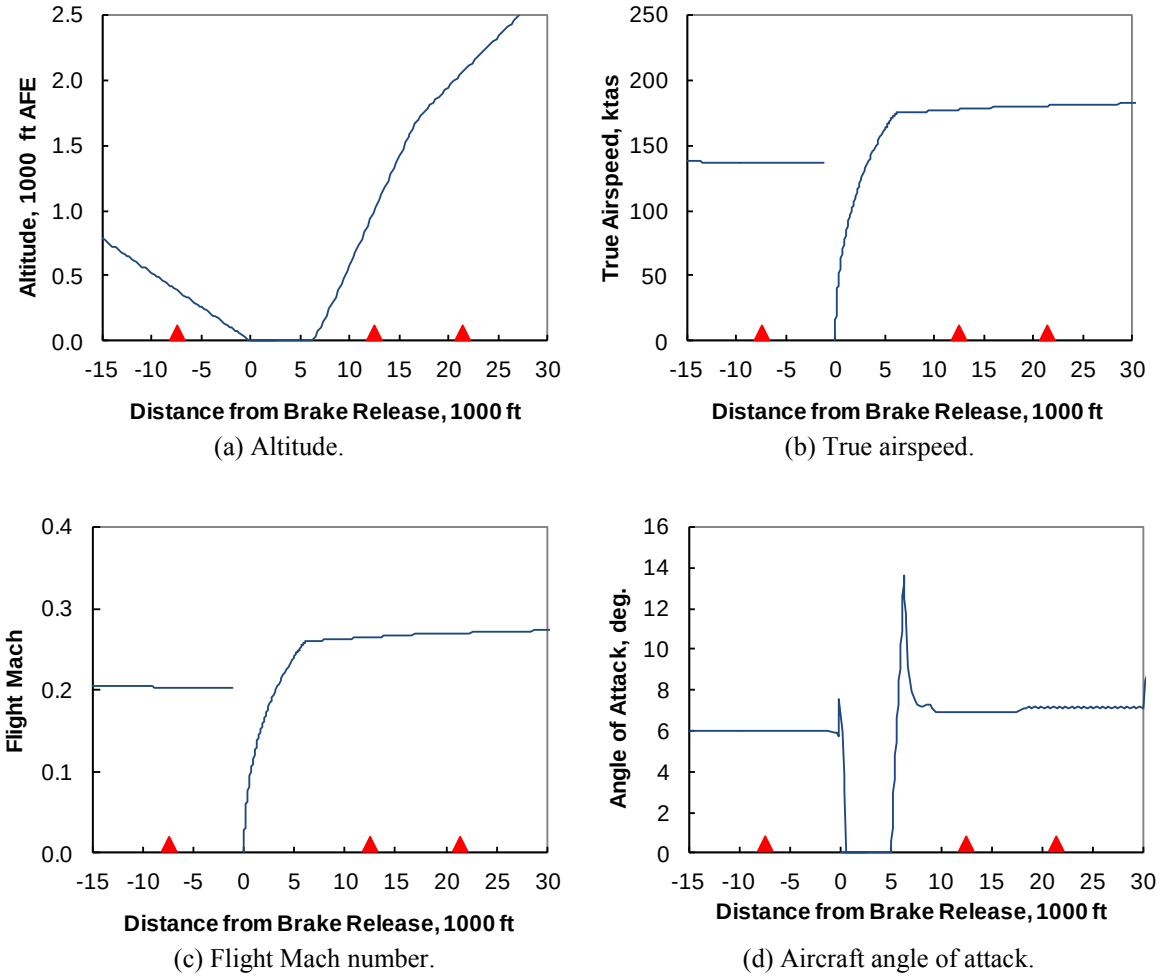


(a) Altitude.

(b) True airspeed.

(c) Flight Mach number.

(d) Aircraft angle of attack.

Figure 12. Takeoff and approach trajectory, aircraft parameters.

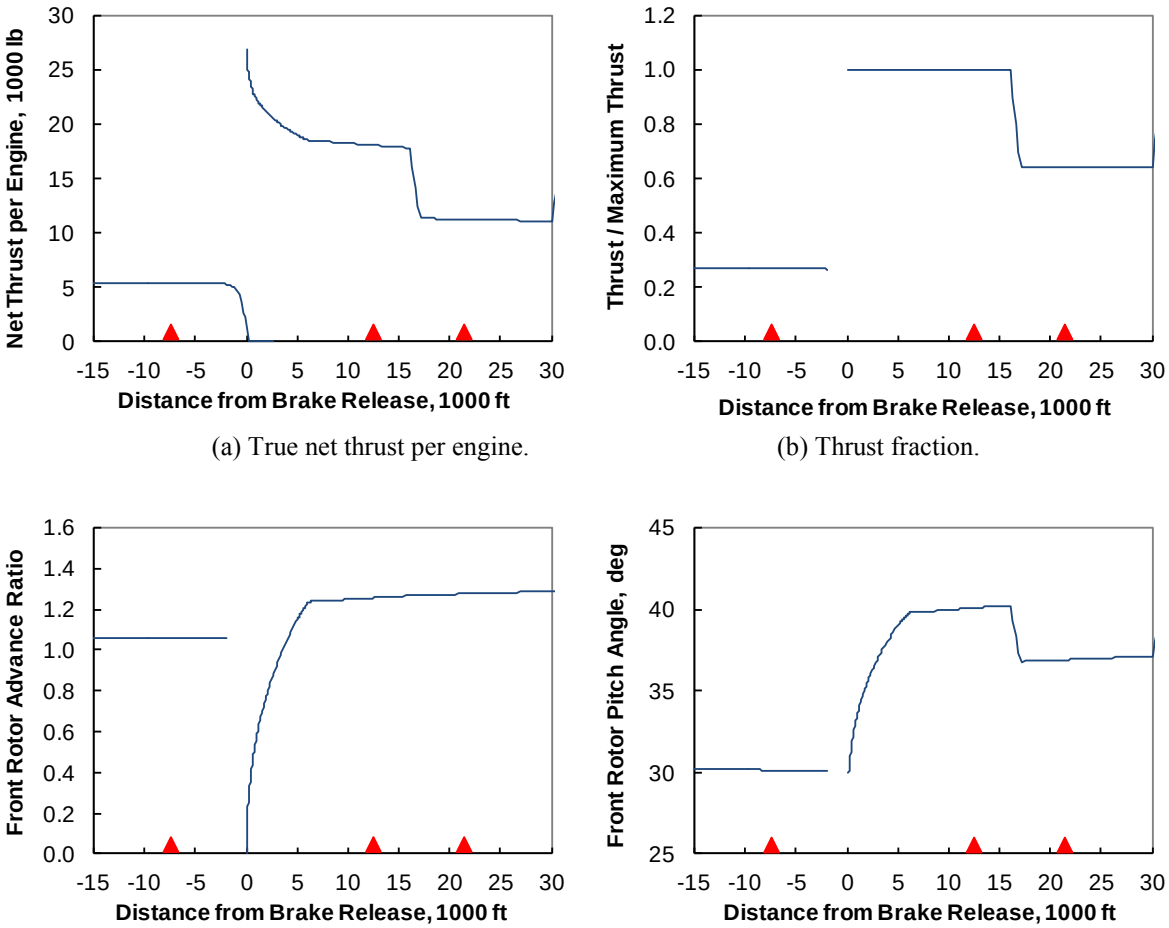


(a) True net thrust per engine.

(b) Thrust fraction.

(c) Front rotor advance ratio.

(d) Front rotor blade pitch angle.

Figure 13. Takeoff and approach trajectory, engine parameters.

### *4.3.2 Noise at Observers*

The EPNL database described in Section 3.3.4 was used to establish reference system noise levels at each observer. This process is illustrated in Figure 14 for the flyover observer. In the chart on the left, the isolated rotor flyover EPNLs at zero inflow angle are correlated with the front rotor tangential tip speed and the scaled thrust per engine. In the tunnel experiments, the tip speed was varied while blade pitch angles were held constant so that ranges of thrust could be investigated. But in practice, the front rotor would be operated at its constant design tip speed, even as the engine is throttled. (The blade pitch angles are flattened by a pitch-change mechanism as power is reduced.) In the chart on the right, the same EPNLs are plotted against the scaled thrust per engine. In this chart, a regression line is created using the locus of minimum EPNLs vs. thrust per engine. In both charts, the thrusts are scaled as described in the Appendix. Either chart may be used to determine the reference EPNL, but correlating the locus of minimum EPNLs against thrust is simpler since the influence of tip speed is removed. The reference system flyover EPNL (81.7 EPNdB) is at the intersection of the airplane cutback thrust per engine (11,270 lbs via the trajectory assessment) and the regression line. A similar process is used to determine

the reference system EPNLs for the approach and lateral observers. The reference system noise levels are adjusted for rotor inflow angle effects and pylon effects as discussed in Section 3.3.5. Such "spreadsheet adjustments" are undesirable – a direct calculation of EPNL is preferred – but accurate rotor source noise prediction methods that include these effects are currently lacking.

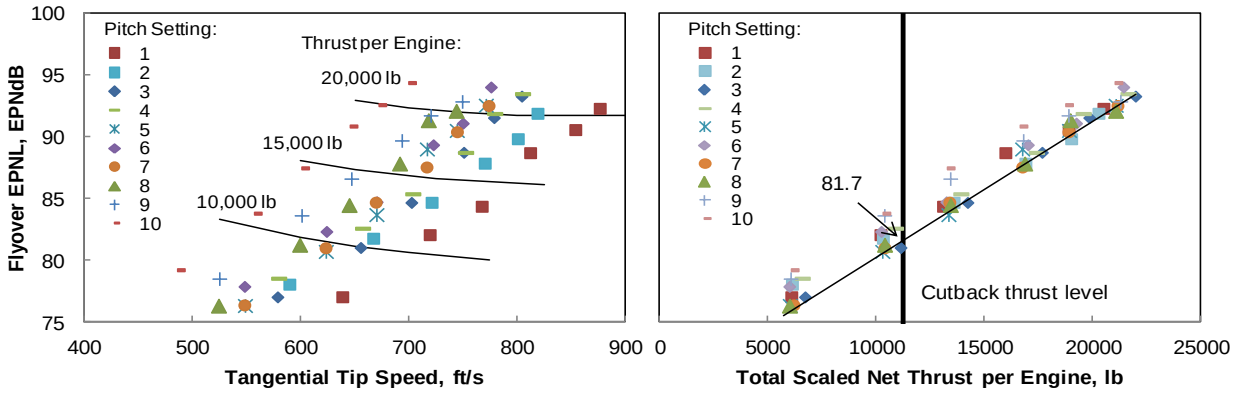


Figure 14. Reference system EPNL for the flyover observer.

The computed lateral, flyover, and approach EPNLs for the NASA open rotor vehicle are shown in Table 4 along with the corresponding Stage 3 limits for an airplane having a maximum takeoff gross weight of 151,300 lbs. For Stage 4 noise certification, the maximum noise level permitted at an individual measurement point is the same as the Stage 3 maximum level. However, Stage 4 aircraft are required to have a margin to Stage 3 of at least 2 EPNdB for any two measurement points combined, and they are required to have a cumulative margin to Stage 3 (all three measurement points combined) of not less than 10 EPNdB. Additionally, "trading" EPNL margins between measurement points is no longer permitted. As seen from Table 4, the noise levels of an airplane using a modern rotor design would meet Stage 4 requirements with a cumulative margin of 12.6 EPNdB.

Table 4. Effective Perceived Noise Levels (EPNdB) for a 151,300 lb Aircraft

| | Approach | Lateral | Flyover | Cumulative |
|---|---|---|---|---|
| Reference Level | 88.7 | 90.2 | 81.7 | 260.5 |
| Inflow Effects | 0.2 | 1.5 | 1.5 | 3.2 |
| Pylon Effects | 0.6 | 0.3 | 0.6 | 1.5 |
| Overall | 89.5 | 92.0 | 83.8 | 265.2 |
| Stage 3 Rule | 100.3 | 96.5 | 91.0 | 287.8 |
| Stage 3 Margin | -10.7 | -4.5 | -7.3 | -22.6 |
| Stage 4 Margin | | | | -12.6 |

## 5.0 Concluding Remarks

An initial capability to assess and evaluate aircraft configurations with open rotor propulsion has been established in NASA. At present, this capability relies heavily on the availability of experimental data for existing rotor designs. Even though open rotor engines are heavy and require airframe accommodations such as additional noise insulation which further increase weight, when applied to an advanced single-aisle airframe the increase in propulsive efficiency results in large reductions in fuel consumption. The benefit relative to an equivalent technology geared turbofan configuration is 18% for short range missions, decreasing to 12% on long range missions. Because the open rotor engine has a higher cruise EI

than the advanced geared turbofan, however, cruise $NO_X$ emissions are higher even though cruise fuel consumption is lower. Despite higher total $NO_X$ emissions, LTO $NO_X$ emissions for the open rotor configuration are 35% less than with an equivalent technology turbofan engine. Noise analysis for the modern low noise rotor design indicates a cumulative Stage 4 margin of 12.6 EPNdB. Development of low noise rotor designs continues beyond the rotors analyzed here, offering the potential for even better performance and lower noise.

## 6.0 References


1. Ethell, J. L.: *Fuel Economy in Aviation*. NASA SP-462, 1983.

2. Bowles, M. D.: *The "Apollo" of Aeronautics: NASA's Aircraft Energy Efficiency Program 1973-1987*. NASA SP-2009-574, 2010.

3. Hager, R. D.; and Vrabel, D.: *Advanced Turboprop Project*. NASA SP-495, 1988.

4. Norris, G.: *Open Return: General Electric and NASA dust off test rigs from 20 years ago*. Aviation Week and Space Technology, July 14, 2008.

5. Norris, G.: *Rig Rolling: Wing tunnel test imminent for Rolls's open rotor rig*. Aviation Week and Space Technology, July 14, 2008.

6. Conlon, J. A.; and Bowles, J. V.: *Application of Advanced High Speed Turboprop Technology for Future Civil Short-Haul Transport Aircraft Design*. AIAA 78-1487, 1978.

7. Blythe, A. A.; and Smith, P.: *Prospects and Problems of Advanced Open Rotors for Commercial Aircraft*. AIAA 85-1191, 1985.

8. U.S. Code of Federal Regulations, Title 14, Chapter I, Part 36. *Noise Standards: Aircraft Type and Airworthiness Certification*.

9. *International Standards and Recommended Practices: Environmental Protection*. Annex 16 to the Convention on International Civil Aviation, Vol. I: Aircraft Noise, 3rd ed., International Civil Aviation Organization (ICAO), Montreal, Canada, July 2008.

10. *Current Market Outlook 2010-2029*. Boeing Commercial Airplanes. 2010.

11. Claus, R.W.; Evans, A.L.; Lytle, J.K., and Nichols, L.D.: *Numerical Propulsion System Simulation*, Computing Systems in Engineering, Vol. 2, No. 4, pp. 357-364, 1991.

12. NPSS User Guide Software Release: NPSS_1.6.5.

13. NPSS Reference Sheets Software Release: NPSS_1.6.5.

14. Onat, E.; and Klees, G.: *A Method to Estimate Weight and Dimensions of Large and Small Gas Turbine Engines.* NASA CR 159481, 1979.

15. Tong, M.T.; Halliwell, I.; Ghosn, L.J.: *A Computer Code for Gas Turbine Engine Weight and Life Estimation*, ASME Journal of Engineering for Gas Turbine and Power, volume 126, no. 2, April 2004.

16. Tong, M.T.; Naylor, B.A.: *An Object-Oriented Computer Code for Aircraft Engine Weight Estimation*, GT2008-50062, ASME Turbo-Expo 2008, June 9-13, 2008.

17. Guynn, M. D.; Berton, J. J.; Fisher, K. L.; Haller, W. J.; Tong, M. T.; and Thurman, D. R.: *Engine Concept Study for an Advanced Single-Aisle Transport*. NASA TM-2009-215784, August 2009.

18. Hendricks, E. S.: *Development of an Open Rotor Cycle Model in NPSS using a Multi-design Point Approach*. GT2011-46694, ASME Turbo-Expo 2011, June 2011.

19. Hendricks, E. S.; and Tong, M. T.: *Performance and Weight Estimates for an Advanced Open Rotor Engine*. AIAA-2012-3911, July 2012.

20. Guynn, M. D.; Berton, J. J.; Fisher, K. L.; Haller, W. J.; Tong, M. T.; and Thurman, D. R.: *Refined Exploration of Turbofan Design Options for an Advanced Single-Aisle Transport*. NASA TM-2011-216883, January 2011.

21. Mann, S. A. E.; and Stuart, C. A.: *Advanced Propulsion through the 1990s: An Airframer's View*. AIAA-85-1192, 1985.

22. McCullers, L.: *Aircraft Configuration Optimization Including Optimized Flight Profiles*. Proceedings of the Symposium on Recent Experiences in Multidisciplinary Analysis and Optimization, NASA CP 2327, April 1984.

23. *MD-90-30 Airplane Characteristics for Airport Planning*. MDC K9099, Boeing Commercial Airplanes, October 2002.

24. Hopkins, H.: *Powerfully Quiet: The McDonnell Douglas MD-90 is likely to meet any Stage 4 requirements*, Flight International, October 26-November 1, 1994.

25. Ardema, M. D.; Chambers, M. C.; Patron, A. P; Hahn, A. S.; Miura, H.; and Moore, M. D.: *Analytical Fuselage* and Wing Weight Estimation of Transport Aircraft. NASA TM 110392, May 1996.

26. http://www.b737.org.uk/flightcontrols.htm. Accessed on 4/11/2011.

27. Henne, P. A.: *MD-90 Transport Aircraft Design*. AIAA-89-2023, 1989.

28. Whitfield, C. E.; Mani, R.; and Gliebe, P. R.: *High Speed Turboprop Aeroacoustic Study, (Counterrotation), Volume I - Model Development*. NASA CR 185241, July 1990.

29. Whitfield, C. E.; Mani, R.; and Gliebe, P. R.: *High Speed Turboprop Aeroacoustic Study, (Counterrotation), Volume II – Computer Programs*. NASA CR 185242, July 1990.

30. Majjigi, M.; and Wojno, J.: *Previous Open Rotor Noise Experience at GE*. X-Noise Open Rotor Technology Seminar, Lausanne, Switzerland; March 18, 2011.

31. NASA Press Release (Vol. 2, Issue 3, March 30, 2009): *GE and NASA Partner on Open Rotor Engine Testing*, http://www.nasa.gov/offices/oce/appel/ask-academy/issues/volume2/AA_2-3_F_ge_rotor.html. Accessed 4/8/2011.

32. *Octave, Half-Octave, Third Octave Band Filters Intended for the Analysis of Sounds and Vibrations*. International Electrotechnical Commission (IEC) Publication 225, 1966.

33. Gillian, R.E.: *Aircraft Noise Prediction Program User's Manual*. NASA TM-84486, 1983.

34. Zorumski, W. E.: *Aircraft Noise Prediction Program Theoretical Manual*. NASA TM-83199, 1981, Parts 1 and 2 (Currently maintained at NASA LaRC by the ANOPP team in electronic format and provided upon request; Latest revision: April, 2011).

35. Rawls, J.: "ACD Module," *ANOPP Theoretical Manual*, ver. 29, NASA Langley Research Center, Hampton, VA, 2011.

36. Emmerling, J.J.; Kazin, S.B.; and Matta, R.K.: *Core Engine Noise Control Program. Volume III, Supplement 1 - Prediction Methods*. FAA-RD-74-125, III-I, Mar. 1976. (Available from DTIC as AD A030 376)

37. Stone, J.R.; Krejsa, E.A.; Clark, B.J.; and Berton, J.J.: *Jet Noise Modeling for Suppressed and Unsuppressed Aircraft in Simulated Flight*. NASA TM-2009-215524, March 2009.

38. Fink, M.R.: *Airframe Noise Prediction Method*. FAA-RD-77-29, March 1977.

39. U.S. Code of Federal Regulations, Title 14, Chapter I, Part 25. *Airworthiness Standards: Transport Category Airplanes*.

40. *Standard Values of Atmospheric Absorption as a Function of Temperature and Humidity*, SAE Aerospace Recommended Practice 866, 1964.

41. Putnam, T.: *Review of Aircraft Noise Propagation*, NASA TM-X-56033, 1975.

42. Delaney, M.; and Bazley, E.: *Acoustical Properties of Fibrous Absorbent Materials*, Applied Acoustics, Vol. 3, No 2, Apr 1970, pp 105-116.

43. *Prediction Method for Lateral Attenuation of Airplane Noise During Takeoff and Landing*, SAE Aerospace Information Report 1751, March 1981.

44. *Environmental Technical Manual on the use of Procedures in the Noise Certification of Aircraft*, Document 9501, 3rd ed., International Civil Aviation Organization (ICAO), Montreal, Canada, 2004.

45. U.S. Code of Federal Regulations, Title 14, Chapter I, Part 34. *Fuel Venting and Exhaust Emission Requirements for Turbine Engine Powered Airplanes*.

# Appendix: Open Rotor Thrust Accounting and Scaling

To make the best use of scale model open rotor acoustic data, a method for scaling measured thrust levels of open rotor test articles to appropriate sizes and flight conditions is needed. Thrust performance, power requirements, and acoustic spectra of scale model open rotor blade sets were measured in the NASA Glenn 9x15-foot Low-Speed Wind Tunnel. The open rotor propulsion rig's data acquisition system provides model-scale rotor thrusts corrected to standard ambient conditions. In order for correct rotor noise levels to be matched to the airplane's thrust demand at each noise certification condition, the thrust levels measured in the wind tunnel experiments must be scaled to full size and to the flight conditions determined by the aircraft trajectory calculations. This thrust-noise matching procedure requires that the thrust levels measured by the open rotor propulsion rig be scaled to the thrust that an actual full-size open rotor propulsion system would produce in flight.

## Dimensional Analysis

A dimensional analysis is often used to gain insight to the behavior of physical systems. Consider a propeller blade of fixed geometry (i.e., the blade airfoil stack and pitch angle are fixed). It is reasonable to assume that the thrust ($F$) acting on the blade is a function of the following physical properties: the propeller diameter ($D$), its rotational speed ($n$), airspeed ($u_o$), as well as the ambient fluid's density ($\rho$), bulk elastic modulus ($K$), dynamic viscosity ($\mu$), static pressure ($P$), and the acceleration due to gravity ($g$). Other dimensional analyses of propellers have included additional (or fewer) properties, but these parameters are more than enough to determine a reasonable set of dependencies. In a dimensional analysis, the force acting on a rotor blade is assumed to take the form of a function:

$$F = f(D^{a_1} n^{a_2} \rho^{a_3} u_o^{a_4} K^{a_5} \mu^{a_6} P^{a_7} g^{a_8})$$

Forcing dimensional homogeneity in the properties of mass ($M$), length ($L$), and time ($T$), the exponents $a_i$ may be related as:

$$[MLT^{-2}] = [(L)^{a_1} (T^{-1})^{a_2} (ML^{-3})^{a_3} (LT^{-1})^{a_4} (ML^{-1}T^{-2})^{a_5} (ML^{-1}T^{-1})^{a_6} (ML^{-1}T^{-2})^{a_7} (LT^{-2})^{a_8}]$$

Equating terms in mass, length, and time, respectively,

$$1 = a_3 + a_5 + a_6 + a_7$$
$$1 = a_1 - 3a_3 + a_4 - a_5 - a_6 - a_7 + a_8$$
$$2 = a_2 + a_4 + 2a_5 + 2a_6 + 2a_7 + 2a_8$$

Solving this system of equations for $a_1$, $a_2$ and $a_3$ results in a meaningful functional relationship and the most sensible solution (in a Buckingham Pi dimensional analysis, $D$, $n$ and $\rho$ would be Buckingham's repeating variables). After rearranging and substituting, $a_1$ through $a_3$ may be written as:

$$a_1 = 4 - a_4 - 2a_5 - 2a_6 - 2a_7 - a_8$$
$$a_2 = 2 - a_4 - 2a_5 - a_6 - 2a_7 - 2a_8$$
$$a_3 = 1 - a_5 - a_6 - a_7$$

And so the rotor thrust is:

$$F = \rho n^2 D^4 f\left\{\left(\frac{u_o}{nD}\right)^{a_4}\left(\frac{K}{\rho n^2 D^2}\right)^{a_5}\left(\frac{\mu}{\rho n D^2}\right)^{a_6}\left(\frac{P}{\rho n^2 D^2}\right)^{a_7}\left(\frac{g}{n^2 D}\right)^{a_8}\right\}$$

But the rotor wheel (tangential) tip speed, $u_T$, is proportional to $nD$, so

$$F = \rho n^2 D^4 f\left\{\left(\frac{u_o}{u_T}\right),\left(\frac{K}{\rho u_T^2}\right),\left(\frac{\mu}{\rho u_T D}\right),\left(\frac{P}{\rho u_T^2}\right),\left(\frac{gD}{u_T^2}\right)\right\}$$

Further, the square of the speed of sound in a medium is $K/\rho$, so the second collection of terms in the brackets is the tangential tip Mach number, $M_T$. Also, a Reynolds number (*Re*) based on the tangential tip speed and with characteristic length $D$ may be defined for the third collection of terms. In addition, the fourth collection of terms is expressed as the cavitation number (*Ca*), and the last terms are expressed as the Froude number (*Fr*).

Finally, the dimensionless term $u_o/u_T = u_o/nD$ is defined as the propeller advance ratio, $J$, resulting in

$$F = \rho n^2 D^4 f\left(J, M_T, Re, Fr, Ca\right)$$

Fluid cavitation and wave effects are generally applicable only to marine propeller performance, so for our purposes *Fr* and *Ca* are omitted. The propeller thrust coefficient is thus defined as

$$C_T \equiv \frac{F}{\rho n^2 D^4} = f\left(J, M_T, Re\right)$$

A similar dimensional analysis may be performed for propeller power (resulting in the propeller power coefficient), but it is unrelated to this discussion of thrust scaling.

$C_T$ remains relatively constant for geometrically similar propellers (i.e., ones in which the airfoil stack definitions, blade pitch angles and blade counts are identical, but may differ in scale), and for aerodynamically similar subsonic propellers (i.e., ones that advance, or corkscrew through the air at the same rate $J$). For minor excursions in altitude and airspeed within the takeoff regime (where compressibility and Reynolds effects are small, and provided $J$ is constant), the flow patterns around the propeller are similar and $F/\rho n^2 D^4$ remains a constant.

## Thrust Scaling in Similitude Conditions

A propeller that maintains geometric and aerodynamic similarity throughout the takeoff and landing flight regime must (by definition) maintain a constant advance ratio. Thus, the tangential tip speed changes at the same rate as the airspeed. Substituting the definitions for the advance ratio ($u_o/nD$) and the

square of the sound speed ($a^2 = \gamma P/\rho$ for a perfect gas, where $\gamma$ is the specific heat ratio) into the thrust equation,

$$F = C_T \rho n^2 D^4 = C_T \rho \left( \frac{u_o}{J} \right)^2 D^2 = C_T \rho a^2 \left( \frac{M_o}{J} \right)^2 D^2 = C_T \gamma P \left( \frac{M_o D}{J} \right)^2$$

where $M_o$ is the flight Mach number. Therefore, thrust scales by:

$$F \sim P M_o^2 D^2$$

The simplest scaling is one where airspeed and tangential tip speed are fixed, and there are changes only in size and altitude. In this case, the thrust scales by:

$$F \sim \rho D^2$$

## Thrust Scaling in Non-Similitude Conditions

In practice, variable-pitch (constant-speed) propellers operate in flight conditions that are decidedly not similar. For practical engine operational and performance reasons, the rotor tangential tip speed (and shaft speed) is held constant. Rotor blade pitch angle is varied as flight conditions change to provide the thrust required. As the airspeed increases from zero at brake release to climbout velocities of well over 150 kts, the advance ratio increases as well. Blade pitch angles must increase with airspeed to maintain peak efficiency. With a constant-speed propeller, scaling thrusts from the wind tunnel Mach number (0.20) to the flight Mach number (often in excess of 0.26) using $PM^2D^2$ scaling is a very poor practice. For example, in going from the wind tunnel condition to the flyover observer flight condition, the thrust multiplier resulting from the Mach-square ratio is as high as 1.8. Without a commensurate increase in rotor tip speed, the rotor thrust would be drastically overpredicted.

Ideally, if there were sufficient wind tunnel data collected at a variety of low-speed flight Mach numbers, a simple empirical thrust correction factor model could be developed. However, nearly all of the open rotor data were collected at a wind tunnel Mach number of 0.20. Therefore, instead, we seek a simple thrust correction multiplier that performs reasonably well for minor excursions in flight conditions in the takeoff regime.

No scaling approach is perfect in non-similitude cases. Something reasonable in the absence of data is desired. From incompressible propeller actuator disk theory, it can be shown that the thrust is proportional to the difference in squares of the exit and entry flow velocities, $u_e^2 - u_o^2$:

$$F = \rho A_{Disk} \frac{u_e^2 - u_o^2}{2}$$

where $A_{Disk}$ is the disk area of the propeller. If changes in $u_e^2 - u_o^2$ are minor for the practical operation of a propeller throughout the takeoff regime, the rotor thrust is proportional to ambient density and diameter squared:

$$F \sim \rho D^2$$

Density ratio scaling is attractive and intuitive since it reacts properly to changes in both altitude and

ambient temperature. Scaling thrust with other altitude-dependent parameters is also possible. One alternative is the static pressure ratio. However, the static pressure ratio changes only with altitude (it is insensitive to changes in ambient temperature). Since thrusts must be scaled from wind tunnel conditions (corrected to international standard atmospheric standard conditions) to warmer standard acoustic day conditions (ISA+18°F), pressure ratio scaling is undesirable.

However, $u_e^2 - u_o^2$ may not truly be constant, so a validation of non-similar density ratio scaling is in order. To examine the validity of density ratio scaling in the takeoff regime, a Monte Carlo simulation was conducted using propeller performance data for a commercially-available general aviation propeller. The reference point from which all other cases were scaled was standard sea level conditions at 130 kts. Altitude, airspeed, and ambient temperature were randomly varied from the reference condition to maximum values of 2500 ft in altitude, 150 kts in airspeed, and ISA+18°F in temperature. Propeller shaft speed was held constant while the shaft power was allowed to vary directly with pressure and inversely with the square root of temperature (constant corrected shaft power). Thrusts and blade pitch angles were outcomes. This analysis replicates the problem of scaling data from wind tunnel conditions to conditions found throughout the takeoff regime.

The results of the Monte Carlo simulation are shown in the figure below. Thrusts obtained using density ratio scaling are indicated by the blue symbols, and thrusts obtained using pressure ratio scaling are indicated by the red symbols. Thrusts scaled from the reference condition using the density ratio compare reasonably well to the actual propeller thrust data. Density ratio scaling results in a smaller average error (about one percent) than pressure ratio scaling (about four percent). Positive error means the scaled thrust is greater than the actual thrust, so this analysis indicates that the scaling process will almost always overpredict the actual thrust. If the scaled thrusts are overpredicted, the process shown in Section 4.3.2 may lead to underprediction of the aircraft noise levels.

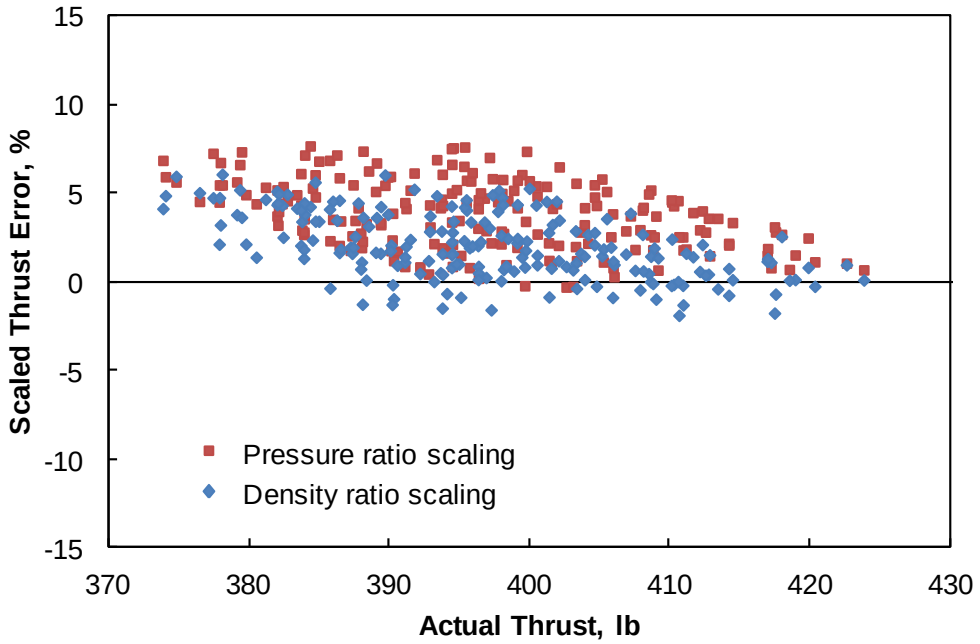

## Thrust Scaling

The following thrust scaling relationship was used for this study:

$$F_{N,\,Total,\,Full-Scale} = F_{Rotor,Rig}\left(\frac{F_{Rotor+Nozz-Ram}}{F_{Rotor\ Alone}}\right)\left(\frac{\rho_{Flight,\,ISA+18F}}{\rho_{SL,\,ISA}}\right)\left(\frac{D_{Full-Scale}}{D_{Rig}}\right)^2$$

where

| | |
|---|---|
| $F_{N,Tot,Full\text{-}Scale}$ | Full scale, total propulsion net thrust per engine |
| $F_{Rotor,Rig}$ | Model scale, open rotor corrected thrust per engine (measured) |
| $F_{Rotor+Nozz\text{-}Ram}$ | Total net thrust (rotor thrust plus core nozzle thrust minus core ram drag) |
| $F_{Rotor\ Alone}$ | Rotor thrust alone |
| $\rho_{Flight,\ ISA+18F}$ | Density at flight altitude, standard acoustic day (ISA+18°F) |
| $\rho_{SL,ISA}$ | Density at sea level, standard day (0.002377 sl/ft$^3$) |
| $(D_{Full\text{-}Scale}/D_{Rig})^2$ | Area scale factor (square of the linear scale factor, model scale to full scale) |

The ratio $F_{Rotor+Nozz\text{-}Ram}$ / $F_{Rotor\ Alone}$ accounts for the small amount of thrust generated by the core nozzle and for the core ram drag. This ratio is determined from the analytical cycle model of the engine. In the model, the pressure exiting the power turbine at the aerodynamic design point at altitude is set so that the core nozzle pressure ratio at sea level is about 1.05. The "nozzle assist" generates a small amount of the total thrust near sea level. For NASA's open rotor propulsion system near sea level, $F_{Rotor+Nozz\text{-}Ram}$ / $F_{Rotor\ Alone}$ = 1.027.

# REPORT DOCUMENTATION PAGE

*Form Approved*
*OMB No. 0704-0188*



| 1. REPORT DATE *(DD-MM-YYYY)* | 2. REPORT TYPE | 3. DATES COVERED *(From - To)* |
|---|---|---|
| 01- 10 - 2012 | Technical Memorandum | |

**4. TITLE AND SUBTITLE**

Performance and Environmental Assessment of an Advanced Aircraft With Open Rotor Propulsion

**5a. CONTRACT NUMBER**

**5b. GRANT NUMBER**

**5c. PROGRAM ELEMENT NUMBER**

**6. AUTHOR(S)**

Guynn, Mark D.; Berton, Jeffrey J.; Haller, William J.; Hendricks, Eric; Tong, Michael T.

**5d. PROJECT NUMBER**

**5e. TASK NUMBER**

**5f. WORK UNIT NUMBER**

561581.02.08.07.42.03

**7. PERFORMING ORGANIZATION NAME(S) AND ADDRESS(ES)**

NASA Langley Research Center
Hampton, VA 23681-2199

**8. PERFORMING ORGANIZATION REPORT NUMBER**

L-20189

**9. SPONSORING/MONITORING AGENCY NAME(S) AND ADDRESS(ES)**

National Aeronautics and Space Administration
Washington, DC 20546-0001

**10. SPONSOR/MONITOR'S ACRONYM(S)**

NASA

**11. SPONSOR/MONITOR'S REPORT NUMBER(S)**

NASA/TM-2012-217772

**12. DISTRIBUTION/AVAILABILITY STATEMENT**

Unclassified - Unlimited
Subject Category 01
Availability: NASA CASI (443) 757-5802

**13. SUPPLEMENTARY NOTES**

**14. ABSTRACT**

Application of high speed, advanced turboprops, or "propfans," to transonic transport aircraft received significant attention during the 1970s and 1980s when fuel efficiency was the driving focus of aeronautical research. Unfortunately, after fuel prices declined sharply there was no longer sufficient motivation to continue maturing this technology. Recent volatility in fuel prices and increasing concern for aviation's environmental impact, however, have renewed interest in unducted, open rotor propulsion. Because of the renewed interest in open rotor propulsion, the lack of publicly available up-to-date studies assessing its benefits, and NASA's focus on reducing fuel consumption, a preliminary aircraft system level study on open rotor propulsion was initiated to inform decisions concerning research in this area. New analysis processes were established to assess the characteristics of open rotor aircraft. These processes were then used to assess the performance, noise, and emissions characteristics of an advanced, single-aisle aircraft using open rotor propulsion. The results of this initial study indicate open rotor engines have the potential to provide significant reductions in fuel consumption and landing-takeoff cycle NOX emissions. Noise analysis of the study configuration indicates that an open rotor aircraft in the single-aisle class would be able to meet current noise regulations with margin.

**15. SUBJECT TERMS**

Aircraft design; Aircraft efficiency; Aircraft noise; Engine design; Open rotor propulsion

| 16. SECURITY CLASSIFICATION OF: | | | 17. LIMITATION OF ABSTRACT | 18. NUMBER OF PAGES | 19a. NAME OF RESPONSIBLE PERSON |
|---|---|---|---|---|---|
| a. REPORT | b. ABSTRACT | c. THIS PAGE | | | STI Help Desk (email: help@sti.nasa.gov) |
| | | | | | 19b. TELEPHONE NUMBER *(Include area code)* |
| U | U | U | UU | 42 | (443) 757-5802 |